Ore Geology Reviews 90 (2017) 148–165

Contents lists available at ScienceDirect

Ore Geology Reviews

journal homepage: www.elsevier.com/locate/oregeo

Metasomatic alteration of chromite from parts of the late Archaean Sittampundi Layered Magmatic Complex (SLC), Tamil Nadu, India

Moumita Talukdar [a,b,*], Sanjoy Sanyal [a], Pulak Sengupta [a]

[a] Department of Geological Sciences, Jadavpur University, Kolkata 700032, India
[b] School of Petroleum Technology, Pandit Deendayal Petroleum University, Gandhinagar 382007, India

ARTICLE INFO

Article history:
Received 5 August 2016
Received in revised form 5 May 2017
Accepted 22 May 2017
Available online 26 May 2017

Keywords:
Archaean chromites
Metamorphism
Element mobility
SLC

ABSTRACT

Chromite deposits associated with layered anorthosite complexes in the Archaean high-grade terranes are rare in the world. The late Archaean Sittampundi Layered Magmatic Complex, Tamil Nadu, India is one of the few such deposits in the world where layers of Fe-Al rich chromites are associated with extremely calcic (An>95) anorthosite. 'Frozen in' magmatic mineralogy of the chromitite and the enclosing anorthosite suggest successive crystallization of chromite + clinopyroxene and chromite + clinopyroxene + anorthite from a hydrous Al-rich basaltic melt that was emplaced in a suprasubduction zone setting. Intense deformation and upper amphibolite facies metamorphism at ~2.45 Ga converted the magmatic assemblages to hitherto unreported hornblende + gedrite + Mg-Al rich spinel ± chlorite bearing assemblages. During metamorphic reconstitution, chromite was pseudomorphically replaced by green spinel in the domains rich in secondary amphiboles. Mass-balance calculation and algebraic analyses of the observed mineralogy suggest that a number of chemical species including chromium became mobile during the formation of spinel pseudomorph in response to infiltration driven metamorphism. Aluminium became mobile in the length scale of chromite grain but remained immobile in the length scale of a thin section.

1. Introduction

Compositional variation of chromite is an important fingerprint to trace the composition of the parental magma from which it was formed, the tectonic setting where the parental magma was emplaced and the intrinsic physicochemical conditions that prevailed during post-solidification changes (reviewed in Ashwal, 1993; Barnes and Roeder, 2001; Berger et al., 2013; Rollinson et al., 2002). Chromitite associated with the metamorphosed layered magmatic complexes of the late Archaean age show unique compositional features (Fe-Al rich chromite associated with anorthite) that distinguish them from the other chromitite deposits that are reported from diverse tectonic settings and over a protracted period of time (Table 1), reviewed in Berger et al., 2013; Dutta et al., 2011; Rollinson et al., 2010, 2002). Preliminary studies from one place of the late Archaean Sittampundi Layered Magmatic Complex (here after SLC) show that SLC is one of such rare occurrences where unusually Fe-Al rich chromite are hosted in ultracalcic anorthosite (Dutta et al., 2011). During superimposed metamorphism at significantly different physicochemical conditions than those prevailed during the magmatic stage, chromite-bearing assemblages underwent compositional and textural changes to restore equilibrium in a new set of conditions (reviewed in Barnes and Roeder, 2001; Rollinson et al., 2010, 2002). Commonly, chromite shows an increase in $Fe^{3+}/(Fe^{3+} + Fe^{2+})$ ratio at constant or variable Cr# ($Cr^{3+}/(Cr^{3+} + Al^{3+})$, reviewed in Barnes and Roeder, 2001; Berger et al., 2013; Mukherjee et al., 2010). Compared to these deposits, chromite shows enrichment in Al and Mg in some deposits (Berger et al., 2013; Candia and Gaspar, 1997; Rollinson et al., 2002). The exact mechanism that triggered the Al-Mg enriched trend in magmatic chromite is poorly understood so far (Berger et al., 2013; Rollinson et al., 2002). Such compositional trend in metamorphic terranes also offers unique opportunity to study the behaviour of Cr and Al during infiltration driven metamorphism.

In this communication we trace the compositional evolution of the rare Fe-Al rich chromitite bands that are enclosed within the highly calcic anorthosite of the late Archaean SLC. Interpreting the vestiges of magmatic assemblages that are preserved in the studied rocks, it is suggested that the magmatic protoliths of the SLC were formed from a hydrous Al-rich basaltic melt that was emplaced in a suprasubduction zone setting. Intense deformation

* Corresponding author at: School of Petroleum Technology, Pandit Deendayal Petroleum University, Gandhinagar 382007, India.
E-mail address: mou.geoju@gmail.com (M. Talukdar).

http://dx.doi.org/10.1016/j.oregeorev.2017.05.021
0169-1368/

Table 1
Archaean chromite deposites in gneissic complex of the world.

Complex	Age of Emplacement	Chromite composition	Plagioclase	Reference
Ujaragssuit nunat Complex	>3.8 Ga	Mg# = 0.06–0.44, Cr# = 0.72–0.96	_	Rollinson et al. (2002)
Fiskenæsset Complex	~2.8 Ga	Mg# = 0.04–0.27, Cr# = 0.46–0.65	An = 0.86–0.90	Rollinson et al. (2010), Ashwal et al. (1989)
Guelb el Azib Complex	~3.5–2.9 Ga	Mg# = 0.1–0.4, Cr# = 0.40–0.75	An = 0.87–0.88	Berger et al. (2013)
Messina Complex	~3.23 Ga	Mg# = 0.25–0.45, Cr# = 0.27–0.50	An = 0.71–0.79	Hor et al. (1975), Barton et al. (1979), Barton (1996)
Sittampundi Layered Complex	~2.9 Ga Bhaskar Rao et al. (1996)	Mg# = 0.23–0.42, Cr# = 0.41–0.53	An = 0.99–1.00	Dutta et al. (2011)
		Mg# = 0.20–0.35, Cr# = 0.28–0.53	An = 0.95–0.99	This study

and infiltration driven metamorphism caused the magmatic chromite to become progressively more aluminous and magnesian. Behaviour and the scale of mobility of Cr and Al during metamorphism of the chromite bearing pyroxenite have been modeled through textural modelling study and the mass balance calculation. Our study demonstrates marked variation in the behaviour of Cr and Al depending upon the scale of observation.

2. Background geology

The Granulite Terrane of South India (GTSI) that fringes the Archaean Dharwar craton to the south have protracted geological history from ~2.9 Ga to 0.45 Ga (reviewed in Brandt et al., 2014; Sajeev et al., 2009; Sengupta et al., 2015; Windley et al., 1981). Northern part of the GTSI is dominated by felsic orthogneisses that contain enclaves of layered magmatic complexes (anorthosite, pyroxenite and mafic rocks, Fig. 1a). The layered magmatic complexes of Sittampundi (hereafter SLC) and Bhawani (BLC) are the two major anorthosite (with variable chromitite bands) bodies that are exposed within felsic orthogneisses (Fig. 1a). The geology of the areas in and around the SLC was first studied in detail by Subramanium (1956) and subsequently by Bhaskar Rao et al. (1996), Chowdhury et al. (2013), Dutta et al. (2011), Ram Mohan et al. (2012) and Sajeev et al. (2009). Extant geological information reveals the following facts about the SLC:

a. Sm-Nd whole rock isochron involving the mafic-ultramafic-anorthosite yield ~2.9 Ga age that is attributed to the timing of protolith formation of the SLC (Bhaskar Rao et al., 1996). This age has been supported by U-Pb age of zircon (~2.9 Ga) collected from the mafic rocks from the adjoining area (Ghosh et al., 2004). Presence of ~2.8 Ga (Brandt et al., 2014) old zircon from the felsic rocks that intruded the SLC seems to be consistent with the ~2.9 Ga age of the SLC. Contrary to these evidences, Ram Mohan et al. (2012) obtained ~2.54 Ga old zircon from the mafic member of the SLC. This

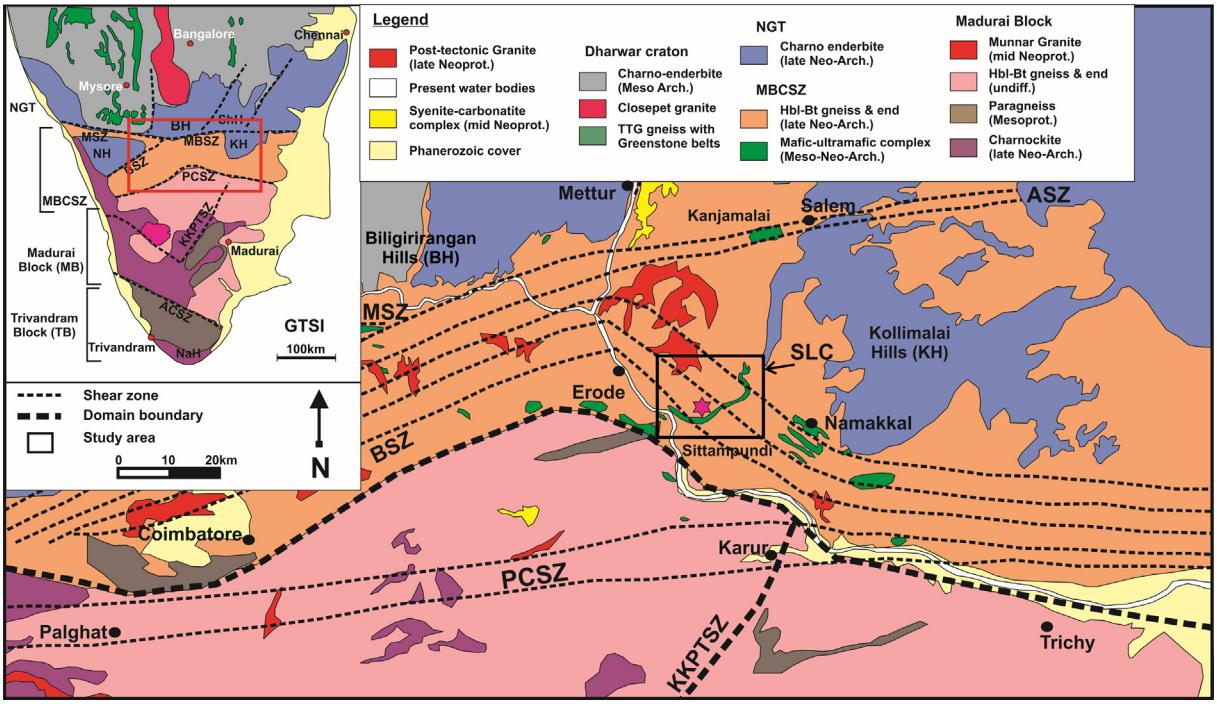

Fig. 1a. Generalized geological map of a section of Moyar-Bhawani-Cauvery shear zone (MBCSZ) from Granulite Terrane of South India (GTSI, shown in the inset with the position of the enlarged section marked in red rectangle) with Northern Granulite Terrane (NGT) in the north and Madurai Block (MB) in the South (modified after the geological map of Tamil Nadu published by Geological survey of India 1995). The Sittampundi Layered complex (SLC) near Sittampundi is marked in black rectangle. The positions of different shear zones like Bhawani shear zone (BSZ), Moyar Shear Zone (MSZ), Palghat–Cauvery Shear Zone (PCSZ), Attur Shear zone (ASZ) and the Karur-Kambam-Painavu-Trichur Shear zone (KKPTSZ) are modified after Brandt et al. (2014).

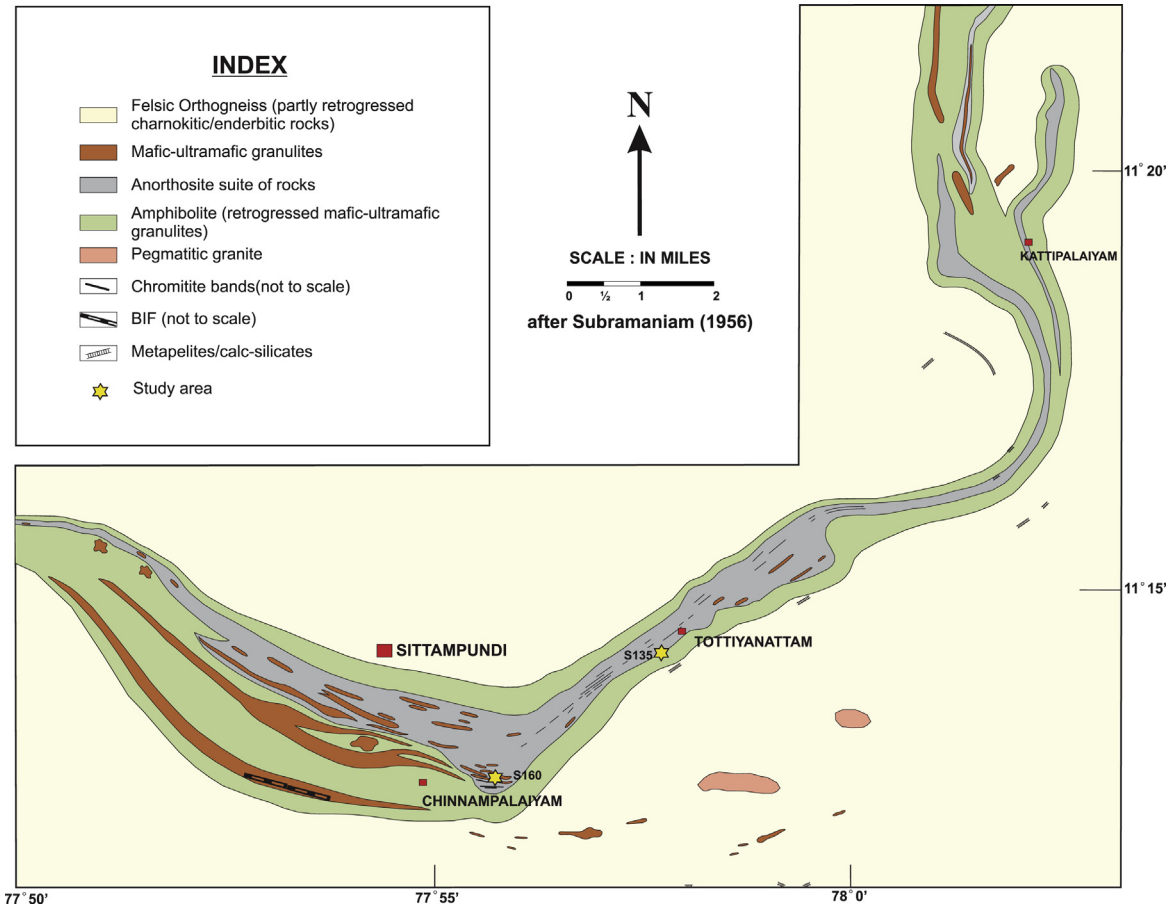

Fig. 1b. Lithological map of the Sittampundi Layered Complex (SLC) with the positions of our study areas, Salem District, Tamil Nadu, India.

has been interpreted to be the age of emplacement of the magmatic members of the SLC. It may be noted that the rocks of the SLC and their extension in the adjoining areas were intruded by voluminous felsic magma (the protoliths of the lithologically dominant felsic orthogneiss, Fig. 1b) that caused significant chemical alteration of the host magmatic rocks (reviewed in Brandt et al., 2014; Dutta et al., 2011). Incidentally, U-Pb dating of zircon from these felsic rocks have yielded ~2.54 Ga age (Ghosh et al., 2004). In view of this observation it is not clear if different parts of the SLC were emplaced at different time or the younger zircon age represent contribution from the younger felsic intrusive. Notwithstanding this problem, an Archaean ancestry of the SLC seems to have been well established. Rocks of the SLC represent with minor Banded Iron Formation (BIF) spatially associated only with the mafic member of the complex which constitute the oldest components of the area. Though anorthosites are restricted to the SLC and BLC, mafic and ultramafic rocks of these complexes and BIF are widespread in the northern part of the GTSI. The felsic orthogneiss that are preponderant in the GTSI show field features that support the view that the protolith of these felsic rocks intruded a basement that is akin to the rocks of the SLC. Presence of the rock ensemble mafic-ultramafic-anorthosite with minor BIF and lack of any older felsic or supracrustal rocks are consistent with the view that the SLC and the related mafic-ultramafic rocks represent a 'fossil' oceanic crust of supra-subduction zone (Brandt et al., 2014; Dutta et al., 2011; Yellappa et al., 2016). Anorthosite and the chromitite bands are considered to be the deeper part whereas the mafic rocks and the BIF represent the upper part of the presumed 'oceanic crust' (Dutta et al., 2011; Yellappa et al., 2016). Geochemistry of the BIF also supports the view that the precursors of the BIF were deposited on an oceanic crust (Yellappa et al., 2016).

b. Anorthosite in the SLC develops the assemblage corundum + hornblende + clinozoisite during peak metamorphism whereas the assemblage garnet-clinopyroxene-plagioclase (GCP) is abundant in the adjoining mafic, ultramafic and the felsic orthogneisses of the studied area (reviewed in Chowdhury et al., 2013; Sengupta et al., 2009). Topological constraint in the system CaO-MgO-Al_2O_3-SiO_2-H_2O and the quantitative geothermobarometry with the GCP (garnet-clinopyroxene-plagioclase) assemblage record pressure >12 kbar and temperature in the range of 700°–800 °C. U-Pb dating of metamorphic zircon from the felsic orthogneiss record ~2.46 Ga which is interpreted to be the age of high pressure metamorphism and the accompanying ductile deformation that affected all the rocks of the SLC and the intrusive felsic rocks (reviewed in Chowdhury et al., 2013). High pressure metamorphism (P > 12 kbar) is ubiquitous in the northern part of the GTSI (reviewed in Brandt et al., 2014)

The studied areas (S160: 11°13.692′ N, 77°53.685′ E and S135: 11°14.106′ N, 77°56.993′ E, Fig. 1b) are located at the southern tip of the SLC where anorthosite and chromitite are conspicuously present. The milk-white anorthosite is spotted with amphiboles containing bands of mafic rock (now amphibolites, Fig. 2a) and clinopyroxene bearing chromitite (mostly altered to

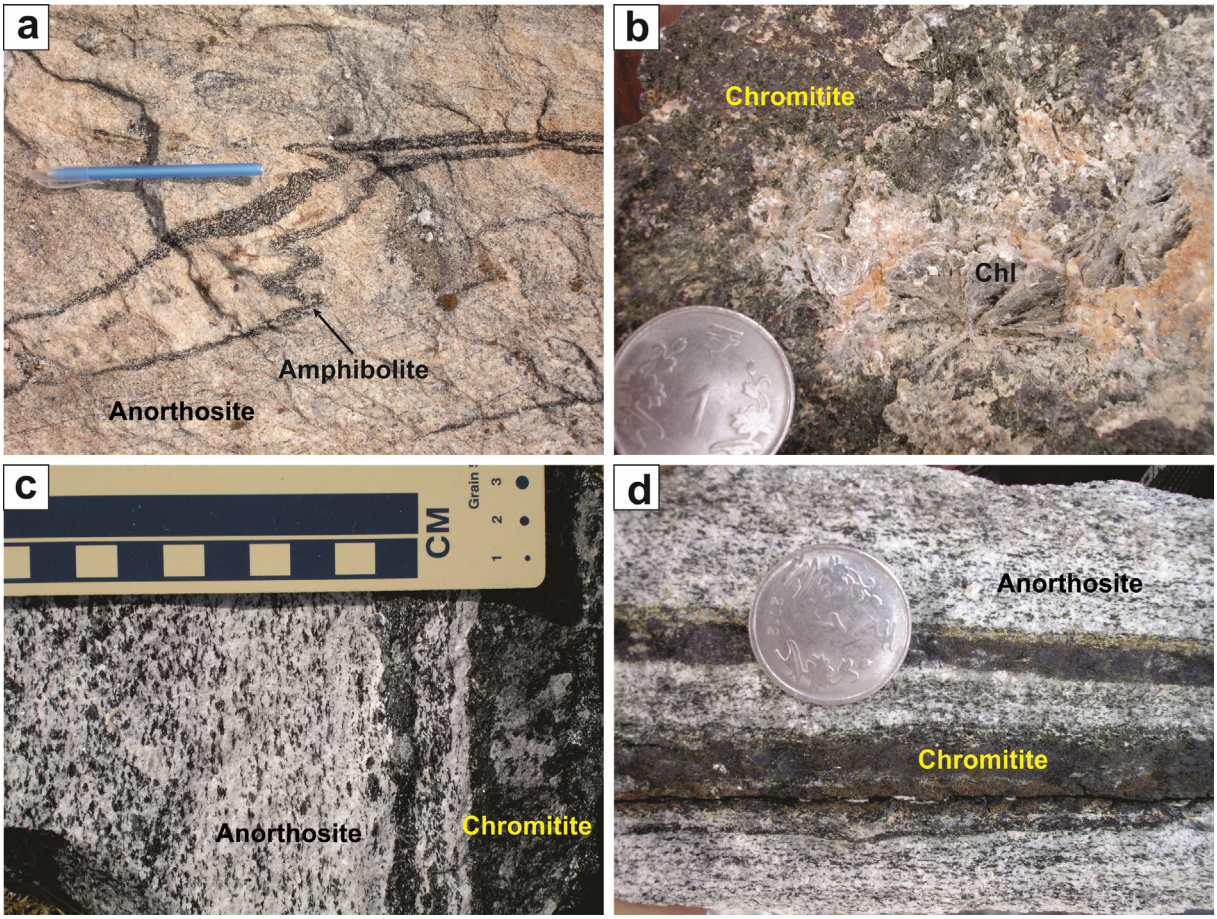

Fig. 2. Field dispositions of anorthosite with amphibolites and chromitite layers. a) Folded amphibolite layers within milky white anorthosite. b) Chlorite flower develop within 7 cm thick hornblende-chromite layer. c) Pinch and swell structure of a cm thick amphibole rich chromitite layers and a 5 cm thick chromitite layer within milky white anorthosite. d) Thin layers of chromitite within anorthosite.

chromite-amphibole-chlorite bearing rock, Fig. 2b–d). Owing to magmatic crystallization and the superposed deformation, large variation of thickness (both laterally as well as vertically) has been noted in the bands of mafic rock and chromitite in anorthosite (Fig. 2b–d). Lack of dimensional arrangements of amphibole and chlorite suggest that these minerals were formed under static condition that prevailed after the cessation of the penetrative deformation.

3. Petrography

In this section the textural features of thin chromitite bands and its host anorthosite are described (Fig. 3a). All the abbreviations that are used in this section are after Kretz (1983) and Siivola and Schmid (2007).

3.1. Anorthosite

Plagioclase constitute more than 80 vol% of the rock and the rest are occupied by variable amounts of clinopyroxene and amphiboles (gedrite and hornblende). Commonly, plagioclase and clinopyroxene form polygonal grains suggesting textural equilibrium was attained (Vernon, 2004). Rarely, relatively larger grains of plagioclase and clinopyroxene show internal strain that are manifested by undulose extinction and bent cleavage traces (Fig. 3b). Haphazard grains of amphibole that develop on the polygonal mosaic of clinopyroxene and plagioclase are devoid of any internal strain (Fig. 3c). Hornblende preferentially occurs along the cleavage traces and partially encloses clinopyroxene (Fig. 3c). Relics of clinopyroxene are present within hornblende (Fig. 3c). This texture is explained by replacement of clinopyroxene by amphibole. In many places, amphibole develops so extensively that polygonal grains of amphibole and plagioclase become the dominant mineralogy of meta-anorthosite (Fig. 3d).

3.2. Chromitite

Significant mineralogical heterogeneity has been observed in the chromitite bands owing to the overprinting metamorphic reconstitution of the pristine magmatic ensembles. In most part of the chromitite bands, chromite (hereafter Chr), amphibole (gedrite and hornblende), chlorite and plagioclase constitute the mineralogy. The haphazardly oriented amphibole grains do not show significant impress of intra-grain strain (Fig. 4a and b). Intergrowth of hornblende and gedrite with planner grain contacts is a common feature of the amphibole-chromite rock (Fig. 4b). Outlines of the Chr that are present in the matrix of amphiboles are invariably rugged and are protruded by the adjoin amphibole grains (Fig. 4a and c). Locally, relics of Chr are present within amphibole grains (Fig. 4a and c). Small plagioclase grains, with irregular outlines, locally present in the matrix of amphibole grains (Fig. 4d and e). Chlorite occurs in two textural modes. Commonly, the flakes of chlorite (<15 vol%) occur in the interstitial spaces formed by hornblende grains (Fig. 4b, d and e). The boundary between hornblende and chlorite are always very sharp that suggests textural and chemical equilibrium between the two minerals (Fig. 4e). Rarely, aggregate

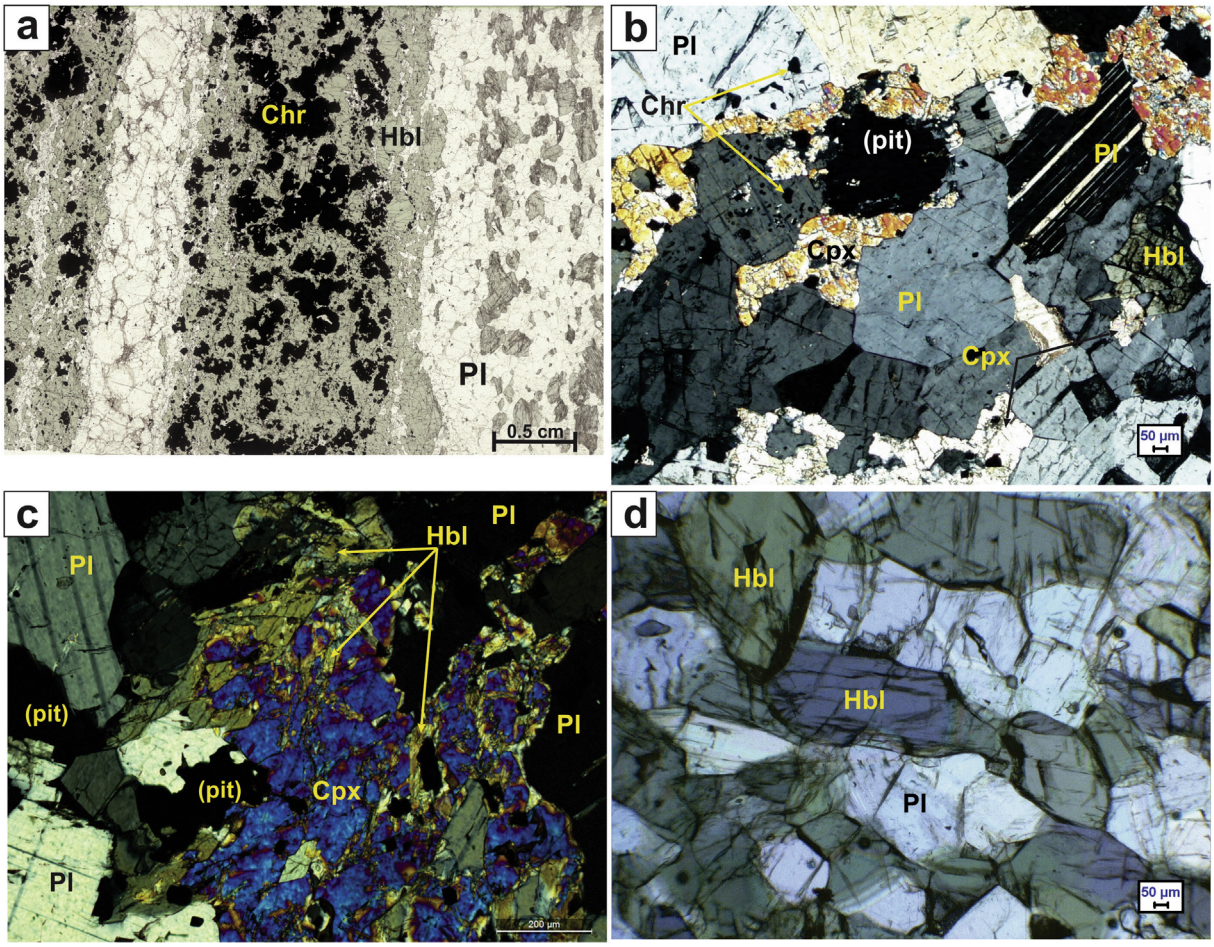

Fig. 3. Microscopic features of anorthosite. a) Thin chromitite layers with amphibole in the matrix hosted within meta-anorthosite under plane polarised light (PPL). Hornblende forms thin rim at the contact of chromitite and adjacent plagioclase of anorthosite. b) Clinopyroxene and plagioclase showing interlocking texture of with few scattered chromite grains within seen under PPL. c) Haphazard hornblende replacing clinopyroxene from grain boundaries and cleavage traces within the initial interlocking texture of clinopyroxene and plagioclase under crossed polars (CPL). d) Polygonal grains of hornblende and plagioclase which constitute the major part of anorthosite rock under PPL.

of haphazardly oriented grains of chlorite form clusters that contain relics of chromites with irregular outlines (Fig. 4f). These textural features are consistent with the fact that (a) amphibole and chlorite were formed after the cessation of any deviatoric stress and (b) amphibole and chlorite formed after Chr. In many domains of the chromitite, amphibole and chlorite constitute less than 15 vol% and the remaining part of the rock is made up of Chr, clinopyroxene and minor plagioclase. Modal proportion of chromite (30–70 vol%) and clinopyroxene (20–60 vol%) in these domains vary widely. Volumetrically minor plagioclase (<15 vol%) occur in the framework made by clinopyroxene and Chr (Figs. 4d, e and 5a–c). The aggregates of clinopyroxene and Chr simulate "cumulus" and 'interlocking' textures that are described from the layered magmatic complexes (Figs. 5a and c, Berger et al., 2013). To our knowledge there exist no published literatures that display clinopyroxene-chromite association in any Archaean deposites. Incidentally, the clinopyroxene-chromite association has been reported from the lunar troctolite (Elardo et al., 2012) and few Cretaceous deposits (Chen et al., 2015; Lenaz et al., 2014; Rollinson and Adetunji, 2015). Subhedral to anhedral grains of chromite show large variation in grain size even in mm size domains (Figs. 4 and 5). Smaller grains of chromite usually concentrate along the margins/interstitial spaces defined by the coarser clinopyroxene grains (Figs. 5a and b). Relics of chromite in clinopyroxene and vice versa are common features in the chromitite (Fig. 5). Unlike the hydrous phases, grains of clinopyroxene, Chr and plagioclase show impress of deformation and deformation induced recrystallization. These are manifested by polygonal grain aggregates, formation of elliptical grains (of Chr), undulose extinction and bent cleavages of clinopyroxene grains (Figs. 4c, f and 5c). Commonly, the grains of clinopyroxene and plagioclase (when present) are variably rimmed and veined by hornblende (Figs. 4d and 5a–c) and gedrite (Fig. 4a). Hornblende forms along the cleavage planes of the deformed clinopyroxene grains (Fig. 5b and c). Corroded relics of clinopyroxene are present within hornblende (Figs. 4d and 5a–c). These textures support the view that (a) Chr + clinopyroxene + plagioclase represent the magmatic mineralogy of the chromitite and (b) amphiboles developed late after the presumed magmatic ensemble underwent intense deformation and recrystallization. In many domains a complete gradation from clinopyroxene + Chr to amphiboles + Chr rocks is noted (Fig. 5c).

In domains, where secondary amphiboles and chlorite are predominant, Chr grains with irregular outline are variably rimmed by green spinel (hereafter GSpl, Fig. 6). GSpl also forms veins and network within and dissect the Chr (Fig. 6c). In places, patches of Chr are present within GSpl (Fig. 6a and b). The boundary between Chr and GSpl is always sharp although a thin layer of greenish brown spinel locally separate Chr from GSpl (Fig. 6b–d). The observed textures are best explained by replacement of the Chr by GSpl. The petrographic features support the view that the 'replacement front' moved from margin to core of the pristine chromite (Fig. 6). The GSpl retains the shape and size of the Chr it replaced (Fig. 6). Chr in clinopyroxene-Chr aggregates is devoid of GSpl rim or vein

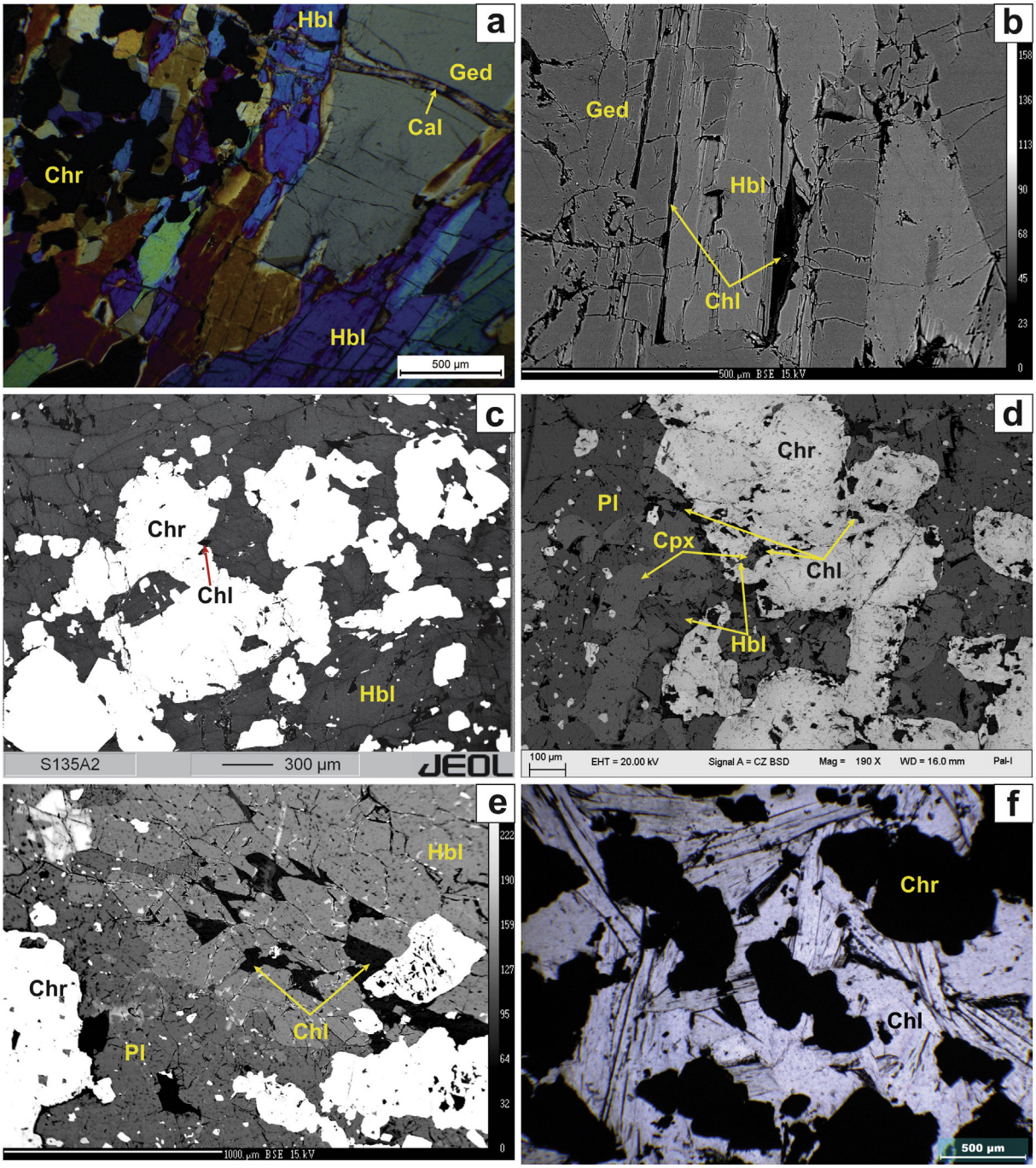

Fig. 4. Microscopic features of chromitite layers. a) Photomicrograph under CPL showing cumulus chromite within matrix of amphibole. Hornblende and gedrite align in a direction. Laths of big gedrite grow with hornblende. A calcite vein crosscut the rock fracturing all early minerals. b) Back scattered electron (BSE) image of hornblende and gedrite grow in gneissose texture in amphibole rich areas with chlorite replacing them from their grain boundaries. c) BSE image of cumulus primary chromite grains in matrix of hornblende with few chlorite grains. d) BSE image of cumulus chromite grains amidst clinopyroxene and plagioclase. Hornblende replaces clinopyroxene through the grain boundary and chlorite replaces these amphiboles from their grain boundaries. e) BSE image showing chlorite growth in the intergranular space of hornblende and amidst plagioclase and primary chromite. f) Primary chromite grains lay as islands within the matrix of chlorite flowers. (All mineral abbreviations are used after Kretz, 1983 and accepted by IUGS, Siivola and Schmid, 2007).

(Figs. 4d and 5c). This feature supports the view that transformation of Chr to GSpl has genetic (and spatial) relation with the hydrous minerals. Similar assemblage is also reported by Nozaka et al. (2016) where they explained the metasomatic growth of green spinel over chromite associated with pargasite and anorthite from Hess Deep Rift troctolites.

4. Mineral chemistry

Representative mineral compositions of the studied rocks are presented in Tables 2–4. Detailed analytical procedure is described in Appendix-A. In the following sections salient compositional features are described.

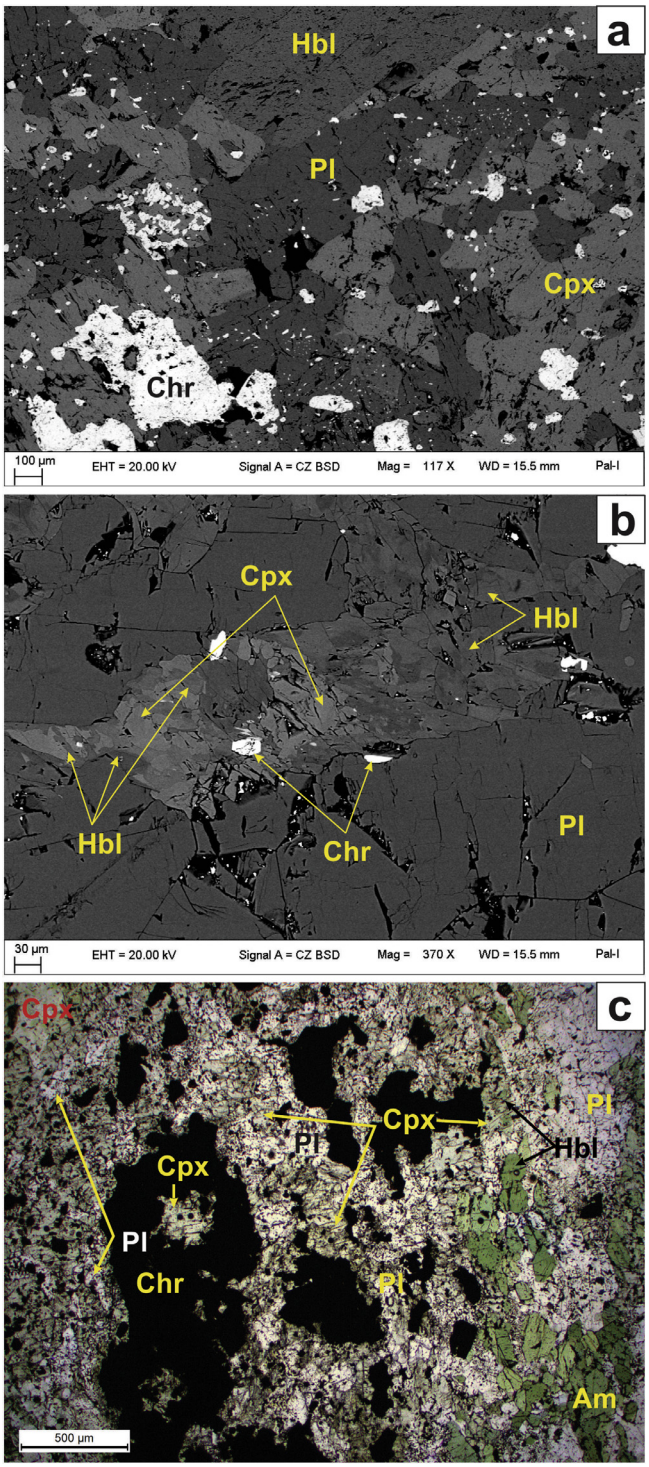

Fig. 5. a) BSE image of chromite grains associated with clinopyroxene and plagioclase having interlocking texture with clinopyroxene relics within chromite and vise versa. Amphibole replaces clinopyroxene and plagioclase. b) BSE image of hornblende replacing a big clinopyroxene grain and plagioclase. c) Photomicrograph of interlocking texture shown by elliptical chromite and clinopyroxene grains where chromite grains are included within clinopyroxene and vise versa under PPL. Hornblende replaces clinopyroxene and plagioclase from one direction of the layer leaving few grains with half pyroxene and half amphibole.

4.1. Chromite and chrome spinel

The variation of the Chr compositional and GSpl are described separately.

4.1.1. Compositions of the Chr

Compositions of Chr are presented in Figs. 7, 8 and Table 2. Chr show significant variation in terms of Al_2O_3 (22.23–32.90 wt%) and Cr_2O_3 (16.70–38.10 wt%) contents with uniformly low TiO_2 ($\leq$0.16 wt%). Fe^{3+} content of Chr shows variation from sample to sample (Fig. 7). Individual grains, however, remains homogeneous with respect to Fe^{3+} content. The Fe^{3+} content of all the analyzed chromite grains are segregated in two clusters in terms of trivalent cations (Fig. 7). In the Cr# (Cr/Cr + Al) vs. Mg# (Mg/Mg + Fe^{2+}) plot the compositions of Chr define an array in which Cr# ($\sim$0.26–0.53) and Mg# (0.22–0.35) shows an inverse relation (Fig. 8). The slope of the compositional array of Chr is similar to the compositional array defined by magmatic chromite reported from all other metamorphosed Archaean chromite deposits associated with layered anorthosite (Fiskenæsset Complex of Greenland, Rollinson et al., 2010; Mangabal complex, Candia and Gaspar, 1997; Guelb el Azib complex and parts of the SLC, Dutta et al., 2011).

4.1.2. Compositions of GSpl

Fig. 9 shows the compositional profile from core to rim of a single chromite grain. It is evident from Fig. 9b that the alteration of Chr is marked by a progressive increase in Mg and Al (towards the rim) that are compensated by a decrease in Fe and Cr. This compositional variation can be explained by simultaneous operation of two exchange vectors $AlCr_{-1}$ and $MgFe_{-1}$. In the Cr# (Cr/Cr + Al) vs. Mg# (Mg/Mg + Fe^{2+}) plot, the compositional profile and the spot analyses of the green spinel (GSpl) define reverse relation between Cr# (0.05–0.15) and Mg# (0.45–0.56, Fig. 10), the compositional change matches with the described compositional change by Nozaka et al. (2016) from troctolites of Hess Deep Rift. The compositional array defined by the green spinel follow the same slope that is defined by the primary chromites of this study (Fig. 10).

4.2. Clinopyroxene

The clinopyroxene grains that are presumed to be a magmatic phase are highly magnesian (Mg# = Mg/(Mg + Fe^{2+})=0.90–0.93, (Table 3) with significant Al_2O_3 (3.65–4.78 wt%) and low Na_2O (<0.10 wt%) and TiO_2 (0.71–1.09 wt%). Individual grains show compositional homogeneity.

4.3. Plagioclase

Extreme calcic nature of plagioclase ($An_{>95}$ with a few data in the range of An_{95-99}) is the characteristic feature of the studied anorthosite (Table 3). Similar highly calcic plagioclase has previously been reported from only a few layered magmatic complex of Archaean age (Table 1), Berger et al., 2013; Dutta et al., 2011; Rollinson et al., 2010).

4.4. Clinoamphibole

The clinoamphiboles (calcic amphibole) are highly aluminous ($\sim$14–16 wt%) with low Cr_2O_3 content ($\leq$0.5 wt%) and TiO_2 content (<1 wt%) and have Na_2O in the range of $\sim$1.67–2.36 wt% (Table 4). The clinoamphibole is the most magnesian mineral in the studied rocks with Mg# = Mg/(Mg + Fe^{2+}) falling in the range 0.88–0.92. The high Mg# of the mineral seems to owe its origin to magnesian clinopyroxene (the latter being replaced by the former). Individual grains do not show any significant compositional variation. According to classification of amphibole (Leake et al., 1997, modified in 2004) the compositions of the amphibole are plotted in the fields of tschermakite and pargasite.

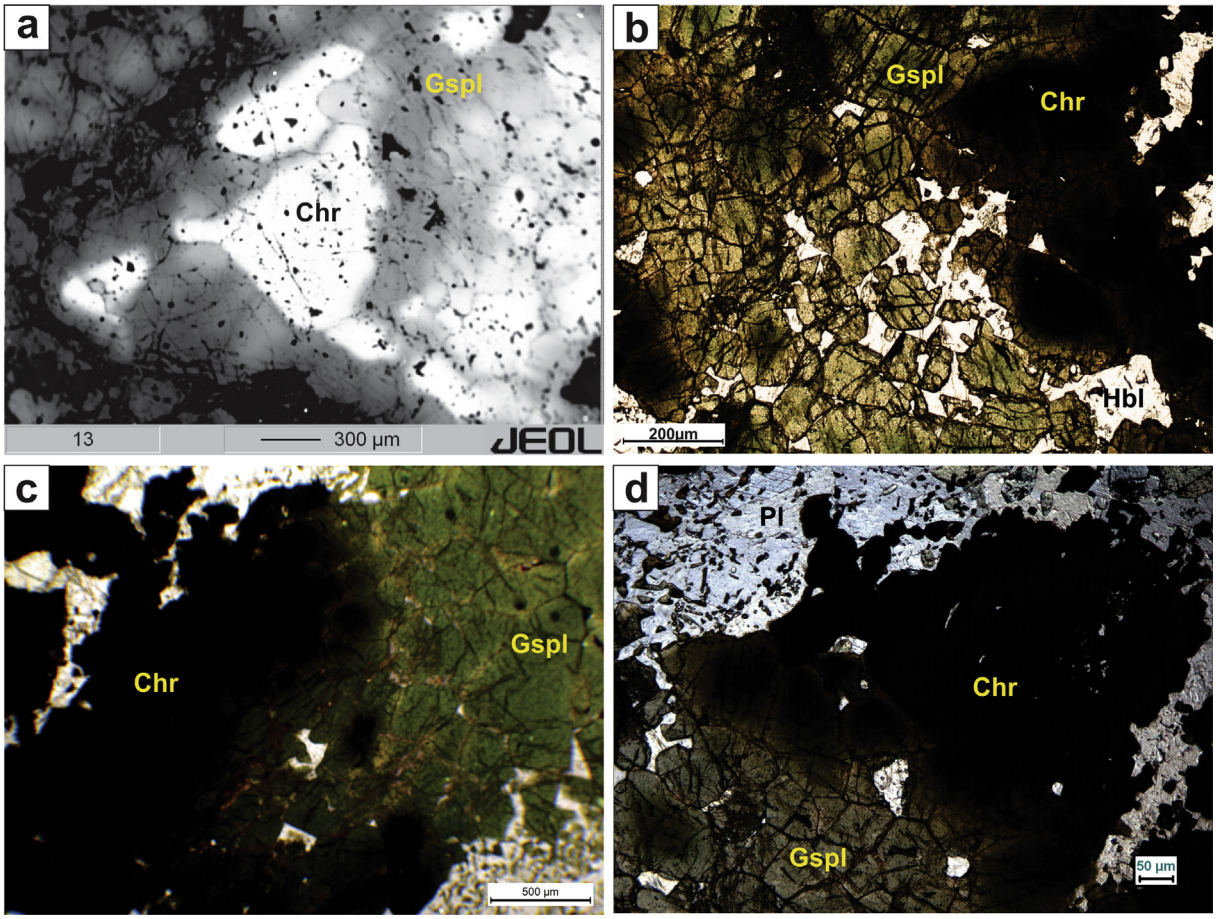

Fig. 6. (a) BSE image and (b–d) photomicrograph under PPL of pseudomorph formation from dark primary chromite (Chr) to green spinel (GSpl).

4.5. Orthoamphibole

According to the classification of Leake et al. (2004, 1997), the composition of the orthoamphibole is plotted in the field of gedrite. Individual grains of orthoamphibole is virtually unzonned with small intergranular compositional variation in terms of Al_2O_3 (18.41–19.10 wt%), Na_2O content (1.67–1.92 wt%) and Mg# (0.87–0.89). Cr_2O_3 and TiO_2 remains very low (0.25–0.34 wt% and 0.16–0.36 wt% respectively, (Table 4).

4.6. Chlorite and calcite

The chlorite is less magnesian with Mg# ($Mg/(Mg + Fe^{2+})$ = 0.80–0.87) than the coexisting amphibole (Table 4). Intriguingly, the chlorite grains that are in direct contact with chromite show low Cr_2O_3 ($\leq$0.6 wt%) and TiO_2 ($\leq$0.1 wt%).

Calcite has virtually end-member compositions.

5. Trace element compositions of plagioclase, amphibole and clinopyroxene

The REE compositions of amphibole, pyroxene and plagioclase were analyzed through LA-ICP-MS and the detail method is discussed in Appendix-A. The list of compositions is given in Table 5. Fig. 11a depicts the chondrite normalized REE patterns of clinopyroxene and amphibole grains where both the minerals mimic the pattern of each other. (Table 5) and Fig. 11a includes two sets of amphibole compositions but both are indistinguishable. In one set amphibole grains partially replace clinopyroxene (denoted by dashed blue lines, Fig. 11a). The other set is taken from rocks where there is no trace of clinopyroxene (amphibole-chromite-plagioclase rock, denoted by bold blue lines, Fig. 11a). However there is general enrichment of LREE in the amphiboles than the clinopyroxene (bold red lines, Fig. 11a) which is noticeable but the HREE do not show any difference.

Fig. 11b and Table 5 show the REE composition of plagioclase from the studied anorthosite (analyzed from portions of anorthosite where anorthite exceeds 80 vol% and the analyzed grains of anorthite are not in contact with other silicate minerals). The Chondrite-normalized REE patterns of the plagioclase of the studied rock matches well with the REE pattern of the plagioclase reported from the Fiskenæsset complex (Rollinson et al., 2010). Plagioclase in the SLC and the Fiskenæsset Complex shows enriched LREE, flat HREE and a conspicuous positive Eu-anomaly (Fig. 11b). However, plagioclase of the Fiskenæsset complex shows higher concentration of LREE than the plagioclase of the studied rocks. This may be related to some difference in the sources rock from which the parental magmas of the two areas were derived.

6. Discussion

It is evident from the foregoing analyses that the studied chromitite within anorthosite records a multitude of textures that were produced during its magmatic crystallization and overprinting metamorphism. The vestiges of the magmatic assemblage clinopyroxene + Chr ± plagioclase are variably replaced by and enclosed in aggregates of secondary hydrous phases (hornblende + gedrite + chlorite). An infiltration driven metamorphism is,

Table 2
Representative microprobe data of chromite (Chr) and green spinel (GSpl).

Mineral	Chr	Chr	Chr	Chr	Chr	GSpl	GSpl	GSpl	GSpl	GSpl	GSpl	GSpl
Points	S135-237	S135-211	S160B-118*# Profile core	S160A-96	S160A-100	S160B-112	S160B-113*	S160B-226	S160B-118# Profile rim	S135-231	S160B-227	S160B-232
SiO_2	0.00	0.00	0.00	0.02	0.03	0.04	0.03	0.02	0.06	0.00	0.02	0.08
TiO_2	0.11	0.16	0.04	0.05	0.04	0.00	0.00	0.02	0.00	0.00	0.01	0.00
Al_2O_3	26.86	22.23	31.63	31.95	32.90	51.96	55.61	43.64	44.29	60.16	43.41	45.11
Cr_2O_3	34.97	38.10	16.70	19.22	18.75	6.58	4.86	10.92	11.30	4.85	10.70	10.00
Fe_2O_3	6.58	7.60	18.35	16.12	15.49	8.52	6.19	12.18	11.58	0.82	12.28	11.31
FeO	29.42	28.41	24.63	25.18	25.18	20.88	19.23	22.50	22.18	21.25	22.53	22.53
MnO	0.26	0.41	0.27	0.33	0.37	0.18	0.20	0.24	0.20	0.04	0.27	0.23
MgO	4.76	4.68	7.56	7.39	7.43	12.34	13.83	10.49	10.85	13.06	10.28	10.69
CaO	0.00	0.02	0.00	0.00	0.00	0.23	0.07	0.00	0.02	0.01	0.00	0.00
Na_2O	0.05	0.00	0.00	0.00	0.00	0.04	0.02	0.00	0.03	0.00	0.02	0.00
Total	103.01	101.60	99.18	100.27	100.19	100.76	100.04	100.02	100.51	100.19	99.53	99.95
Oxygen basis = 4												
Si	0.000	0.000	0.000	0.001	0.001	0.001	0.001	0.001	0.002	0.000	0.001	0.002
Ti	0.003	0.004	0.001	0.001	0.001	0.000	0.000	0.000	0.000	0.000	0.000	0.000
Al	0.984	0.842	1.159	1.157	1.186	1.681	1.770	1.484	1.493	1.883	1.485	1.524
Cr	0.860	0.967	0.410	0.467	0.453	0.143	0.104	0.249	0.256	0.102	0.246	0.227
Fe^{+3}	0.154	0.184	0.429	0.373	0.357	0.176	0.126	0.265	0.249	0.016	0.268	0.244
Fe^{+2}	0.765	0.763	0.640	0.647	0.644	0.479	0.434	0.543	0.531	0.472	0.547	0.540
Mn	0.007	0.011	0.007	0.009	0.010	0.004	0.005	0.006	0.005	0.001	0.007	0.006
Mg	0.221	0.224	0.351	0.339	0.339	0.505	0.557	0.452	0.463	0.517	0.445	0.457
Ca	0.000	0.001	0.000	0.000	0.000	0.007	0.002	0.000	0.001	0.000	0.000	0.000
Na	0.003	0.000	0.000	0.000	0.000	0.002	0.001	0.000	0.001	0.000	0.001	0.000
Total	3.000	3.000	3.000	3.000	3.000	3.000	3.000	3.000	3.000	3.000	3.000	3.000
Cr#	0.430	0.486	0.205	0.234	0.227	0.071	0.052	0.125	0.128	0.051	0.123	0.114
Al#	0.493	0.422	0.580	0.580	0.594	0.841	0.885	0.743	0.747	0.941	0.743	0.764
Fe^{3+}#	0.077	0.092	0.215	0.187	0.179	0.088	0.063	0.132	0.125	0.008	0.134	0.122
Mg#	0.224	0.227	0.354	0.344	0.345	0.513	0.562	0.454	0.466	0.523	0.449	0.458

*Data used for reaction modelling.
Fe^{+3} and Fe^{2+} are done by charge balanced method described in Sengupta et al. (2009).
Cr# = Cr/(Cr + Al); Al# = Al/(Cr + Al + Fe^{3+}); Fe^{3+}# = Fe^{3+}/(Cr + Al + Fe^{3+}); Mg# = Mg/(Mg+Fe^{2+}).
Data used for mass balance calculation.

Table 3
Representative microprobe data of clinopyroxene (Cpx) and plagioclase (Pl).

Mineral	Cpx				Mineral	Pl							
Point	S135-213	S135-215*	S135-218	S135-222	Point	S135-939	S135-941	S135-7	S135-8	S135-14	S160-18*	S160B-101	S160B-102
SiO_2	49.28	49.58	49.73	51.12	SiO_2	42.12	42.73	43.02	43.17	42.34	43.15	43.36	43.36
TiO_2	0.71	1.09	0.71	0.75	TiO_2	0.00	0.00	0.00	0.00	0.00	0.06	0.02	0.01
$Al2O_3$	4.45	4.78	3.65	4.15	Al_2O_3	36.46	36.18	36.44	37.09	35.92	36.15	35.11	34.74
$Cr2O_3$	0.38	0.46	0.28	0.35	Cr_2O_3	0.08	0.00	0.01	0.11	0.00	0.00	0.02	0.01
FeO	3.86	3.77	3.58	3.70	MgO	0.03	0.00	0.00	0.02	0.04	0.02	0.00	0.00
MnO	0.10	0.04	0.00	0.03	FeO	0.03	0.04	0.12	0.05	0.02	0.13	0.38	0.04
MgO	14.40	14.42	14.70	14.88	CaO	20.33	20.05	19.90	20.26	19.92	20.10	19.50	19.37
CaO	24.64	24.85	24.65	24.94	MnO	0.00	0.14	0.00	0.00	0.00	0.00	0.00	0.00
Na_2O	0.08	0.04	0.06	0.05	Na_2O	0.13	0.19	0.32	0.32	0.38	0.35	0.57	0.54
K_2O	0.00	0.03	0.00	0.01	K_2O	0.00	0.01	0.02	0.00	0.00	0.00	0.00	0.00
Total	97.91	99.05	97.36	99.98	Total	99.18	99.34	99.83	101.02	98.62	99.96	98.96	98.10
Oxygen basis = 6					Oxygen basis = 8								
Si	1.847	1.840	1.873	1.876	Si	1.973	1.996	1.998	1.983	1.993	2.003	2.033	2.046
Ti	0.020	0.030	0.020	0.021	Ti	0.000	0.000	0.000	0.000	0.000	0.002	0.001	0.000
Al	0.197	0.209	0.162	0.179	Al	2.013	1.992	1.995	2.009	1.993	1.978	1.941	1.933
Cr	0.011	0.013	0.008	0.010	Cr	0.003	0.000	0.000	0.004	0.000	0.000	0.001	0.000
Fe^{3+}	0.062	0.042	0.048	0.021	Mg	0.002	0.000	0.000	0.001	0.003	0.001	0.000	0.000
Fe^{2+}	0.059	0.075	0.064	0.093	Fe^{2+}	0.001	0.002	0.005	0.002	0.001	0.005	0.015	0.002
Mn	0.003	0.001	0.000	0.001	Ca	1.020	1.004	0.990	0.997	1.005	1.000	0.979	0.980
Mg	0.805	0.797	0.825	0.814	Mn	0.000	0.006	0.000	0.000	0.000	0.000	0.000	0.000
Ca	0.990	0.988	0.995	0.981	Na	0.012	0.017	0.029	0.029	0.035	0.032	0.052	0.050
Na	0.006	0.003	0.004	0.004	K	0.000	0.001	0.001	0.000	0.000	0.000	0.000	0.000
K	0.000	0.001	0.000	0.000	Total	5.025	5.017	5.020	5.025	5.028	5.021	5.021	5.012
Total	4.000	4.000	4.000	4.000									
					X_{An}	0.99	0.98	0.97	0.97	0.97	0.97	0.95	0.95
Mg#	0.93	0.91	0.93	0.90									
Wo%	53.42	53.11	52.78	51.94									
Ens%	43.41	42.87	43.79	43.13									
Fs%	3.17	4.02	3.42	4.92									
AlCaTs	0.06	0.08	0.05	0.08									

*Data used for reaction modelling.
Mg# = (Mg/(Mg + Fe^{2+}).
X_{An} = Ca/(Ca + Na + K).

Table 4
Representative microprobe data of clino-amphibole (Cam), *ortho*-amphibole (Oam) and chlorite (Chl).

Mineral	Cam					Oam			Mineral	Chl				
Point No.	S135-17	S135-22	S160B 19*	S160B-230	S160B-231	S135-24	S135-27	S160B-21*	Point No.	S135-933	S135-5	S160B-12*	S160B-236	S160B-237
Species	Ts	Ts	Ts	Prg	Ts	Ged	Ged	Ged						
SiO_2	43.41	45.21	43.95	44.65	44.35	42.71	43.72	42.81	SiO_2	27.09	28.87	27.13	28.03	28.10
TiO_2	0.97	0.33	0.84	0.11	0.10	0.22	0.36	0.16	TiO_2	0.00	0.05	0.11	0.00	0.02
Al_2O_3	15.97	14.95	15.67	14.30	14.53	19.10	18.41	18.96	Al_2O_3	24.66	24.72	22.04	20.18	20.14
Cr_2O_3	0.74	0.48	0.17	0.49	0.47	0.26	0.25	0.34	Cr_2O_3	0.00	0.54	0.41	0.52	0.60
FeO	7.23	7.02	6.95	7.64	7.15	10.71	10.65	10.32	MgO	26.81	26.31	28.79	25.54	25.23
MnO	0.08	0.05	0.12	0.12	0.10	0.10	0.11	0.11	FeO	6.83	8.20	8.95	11.07	10.99
MgO	15.16	16.63	16.27	16.21	15.69	21.46	21.36	21.17	CaO	0.11	0.07	0.00	0.05	0.05
CaO	11.69	11.54	11.45	10.95	11.07	0.94	0.78	0.90	MnO	0.09	0.02	0.05	0.05	0.03
Na_2O	1.68	1.67	1.84	2.36	2.13	1.82	1.92	1.67	Na_2O	0.17	0.02	0.03	0.00	0.01
K_2O	0.08	0.04	0.09	0.11	0.06	0.00	0.00	0.00	K_2O	0.05	0.00	0.02	0.00	0.00
Total	97.01	97.92	97.35	96.95	95.65	97.32	97.56	96.44	Total	85.81	88.80	87.53	85.46	85.16
Oxygen basis = 23 + H_2O									Oxygen basis = 14 + $4H_2O$					
Si	6.165	6.323	6.198	6.353	6.375	5.914	6.043	5.973	Si	2.637	2.725	2.631	2.81	2.82
Ti	0.104	0.035	0.089	0.012	0.011	0.023	0.037	0.017	Ti	0.000	0.004	0.008	0.00	0.00
Al	2.674	2.465	2.605	2.398	2.462	3.118	3.000	3.119	Al	2.829	2.750	2.520	2.38	2.38
Cr	0.083	0.053	0.019	0.055	0.053	0.028	0.027	0.038	Cr	0.000	0.040	0.031	0.04	0.05
Fe^{3+}	0.463	0.508	0.493	0.450	0.426	0.683	0.566	0.611	Mg	3.889	3.700	4.161	3.81	3.78
Fe^{2+}	0.396	0.314	0.327	0.459	0.434	0.558	0.665	0.593	Fe^{2+}	0.556	0.647	0.726	0.93	0.92
Mn	0.010	0.006	0.014	0.015	0.012	0.012	0.013	0.013	Ca	0.011	0.007	0.000	0.01	0.01
Mg	3.209	3.466	3.419	3.438	3.362	4.429	4.400	4.402	Mn	0.007	0.002	0.004	0.00	0.00
Ca	1.779	1.729	1.730	1.668	1.706	0.139	0.116	0.135	Na	0.032	0.004	0.006	0.00	0.00
Na	0.463	0.453	0.503	0.652	0.594	0.489	0.515	0.452	K	0.006	0.000	0.002	0.00	0.00
K	0.014	0.007	0.016	0.020	0.012	0.000	0.000	0.000	Total	9.968	9.878	10.089	9.98	9.96
Total	15.360	15.359	15.414	15.520	15.446	15.393	15.381	15.352						
									Mg#	0.87	0.85	0.85	0.80	0.80
Mg#	0.89	0.92	0.91	0.88	0.89	0.89	0.87	0.88						

*Data used for reaction modelling.
Cation recalculation after Leake et al., 1997 (modified in 2004).
Mg# = (Mg/(Mg + Fe^{2+}).

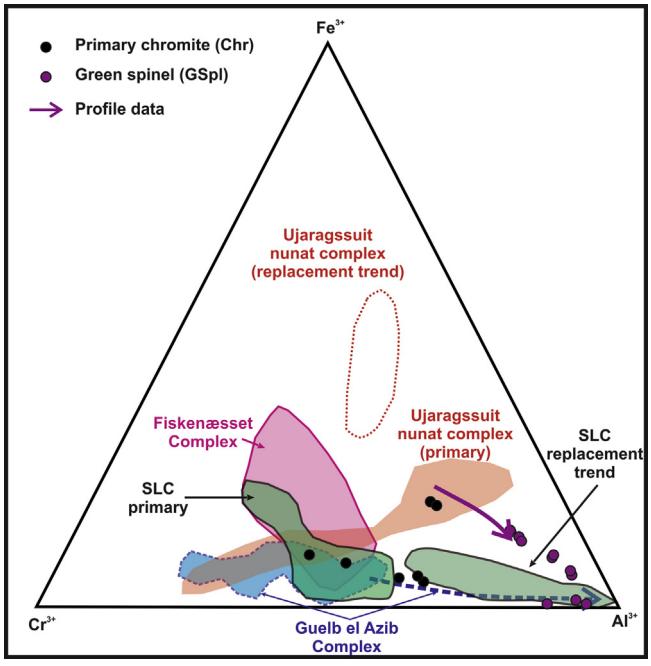

Fig. 7. Triangular plot showing the Cr–Al–Fe^{3+} variation in the chromites and spinels of this study compared with the chromites already reported from SLC (Dutta et al., 2011), Ujaragssuit nuant Complex (Rollinson et al., 2002), Fiskenæsset complex (Rollinson et al., 2010) and Guelb el Azib complex (Berger et al., 2013).

therefore, invoked to explain the formation of hydrous secondary phases at the expense of the anhydrous magmatic assemblages. Proximal to the secondary hydrous minerals replacement of Chr by GSpl appears to be pseudomorphic, preserving external shape and dimension of parent Chr (Fig. 6).

Interpretations of the observed textural relations and the compositional variation of the altered chromite in the studied chromitite are presented under the following heading.

6.1. Probable igneous character of chromitite-anorthosite of SLC

Superposed deformation and intense metamorphism have obliterated most of the magmatic imprint of the SLC. Nevertheless, certain 'frozen in' magmatic features of the studied rocks are presented below to get a perspective of the alteration of chromite in the studied rocks. These features are:

1. Rhythmic alternation of chromitite and anorthosite (and also chromite-rich and clinopyroxene-rich alternation in chromitite), mineralogy and presence of relict 'cumulus' texture in chromitite are consistent with in situ magmatic crystallization as recorded from other layered magmatic complexes (Rollinson et al., 2010, 2002; Stowe, 1994). Studies have shown that the mafic-ultramafic-anorthosite of the SLC are co-genetic and their magmatic protoliths were extracted from a depleted mantle at 2.94 Ga (Bhaskar Rao et al., 1996).
2. Experimental studies of Feig et al. (2006) show that in order to suppress crystallization of orthopyroxene from a high aluminium basaltic melt at temperature >1100 °C, the depth of crystallization should not be much above 2 kbar. Furthermore, amphibole becomes a liquidous phase from such a melt if the temperature drops below 1000 °C at pressure ~2 kbar (Feig et al., 2006). These evidences support that the magmatic crystallization of the studied rocks occurred at shallow depth (<10 km) and at temperature >1000 °C to suppress the

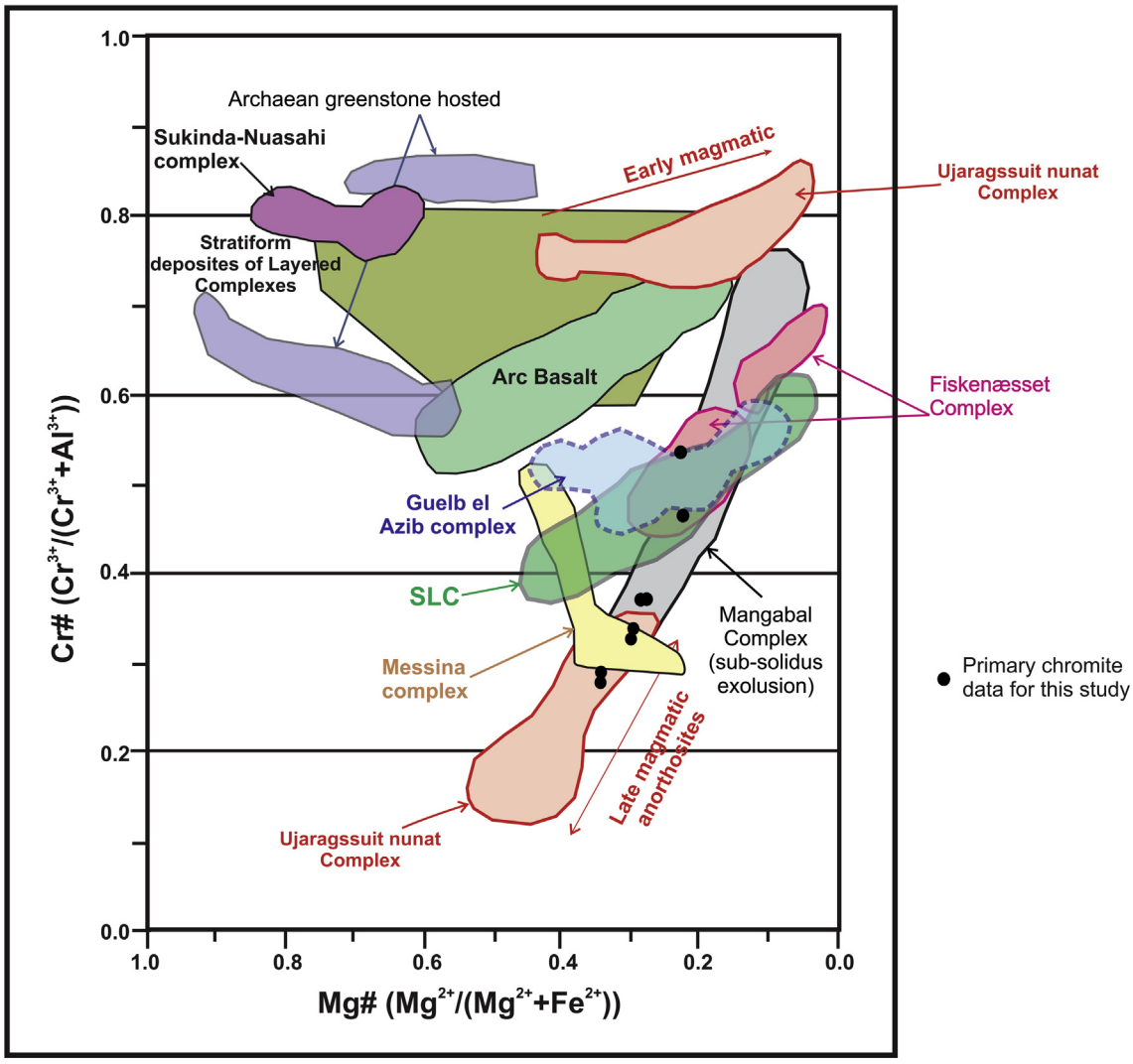

Fig. 8. The primary chromite compositions of this study are plotted in Cr# (Cr/(Cr + Al) vs. Mg# (Mg/(Mg + Fe^{2+}) space with few other chromites deposits reported from Archaean age. The Archaean greenstone hosted chromites reported by Stowe (1994), Sukinda-Nuasahi Complex by Mondal et al. (2006), Ujaragssuit nuant Complex by Rollinson et al. (2002), Fiskenæsset complex by Rollinson et al. (2010), Messina Complex by Hor et al. (1975), Mangabal Complex by Candia and Gaspar (1997), Guelb el Azib complex by Berger et al. (2013), Fiskenæsset complex reported by Rollinson et al. (2010) and the Sittampundi Layered complex (SLC) was been previously reported by Dutta et al. (2011). Chromites of the stratiform deposits of layered complexes (Barnes and Roeder, 2001) are also plotted for comparison.

crystallization of primary amphibole and orthopyroxene. That the SLC was emplaced at shallow depth has also been suggested by Dutta et al. (2011).

3. Compositional spread of chromite in the chromitite (Fig. 8), composition and the pattern of REE (particularly the MREE and HREE) of plagioclase reported in this study (Fig. 11) bear marked resemblance with the chromite and plagioclase compositions reported from the late Archaean Fiskenæsset complex of Greenland (Rollinson et al., 2010). However, some plagioclase grains of the Fiskenæsset complex are slightly enriched in LREE with respect to the plagioclase grains of the SLC (Fig. 11b). This may reflect a difference of parental melt composition with or without post magmatic changes. LREE being more mobile (relative to MREE and HREE), a small change in physicochemical conditions during magmatic or post-magmatic stages would lead to a significant change in LREE concentration (Rollinson, 1993). Compared to the chromite compositions of chromitite (±anorthosite) that are presumed to have formed in the post Archaean arc setting, the chromite and plagioclase of the chromitite-anorthosite of the SLC are distinctly rich in Fe-Al (Fig. 8) and Ca respectively (Table 1). Our interpretation, therefore, corroborate the views of Rollinson et al. (2010) and Dutta et al. (2011) that a hydrous basaltic melt could be the likely candidate that triggered the growth of unusually Fe-Al rich chromite and highly calcic plagioclase.
4. Number of experimental studies (Berndt et al., 2005; Feig et al., 2006; Sisson and Grove, 1993; Takagi et al., 2005) coupled with natural observations (reviewed in Dutta et al., 2011) demonstrate that highly calcic plagioclase can crystallize from basaltic melts that are hydrous in nature. Total pressure has little or no effect on the partitioning coefficient of Na-Ca between plagioclase and melt (reviewed in Dutta et al., 2011). Hydrous melts also help crystallization of Fe-Al chromite (Matveev and Ballhaus, 2002). In view of these evidences, it is presumed that parental melt of the studied chromitite bearing anorthosite were hydrous in nature.

Combining all the evidences a generalized crystallization history of the studied rock appears to be the following:

A batch of hydrous basaltic liquid fractionated olivine and pyroxene and became rich in Al, Cr, Fe and H_2O. Crystallization of plagioclase and minor clinopyroxene from the evolved hydrous

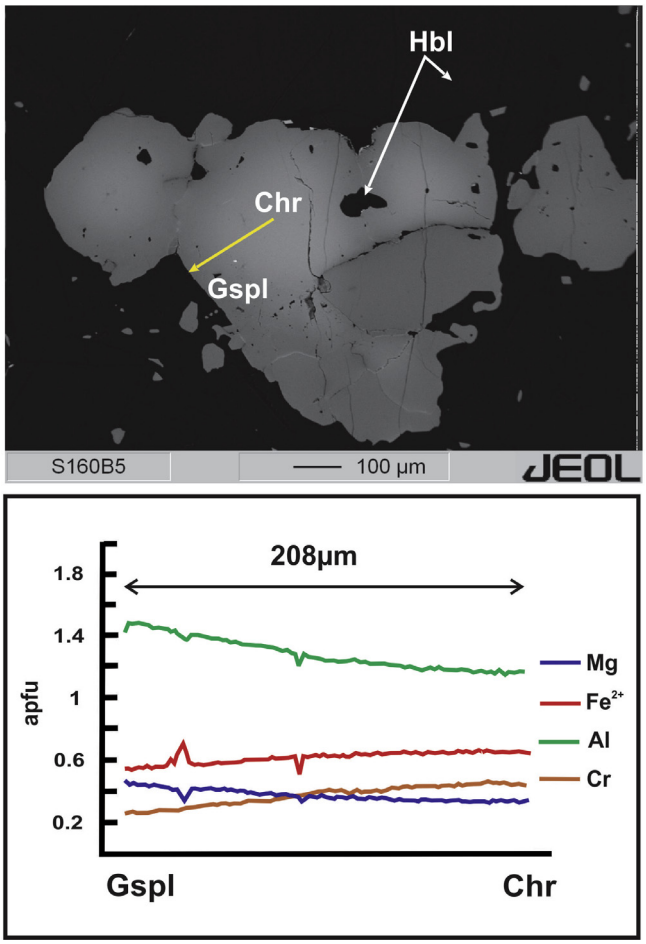

Fig. 9. a) BSE image of the chromite grain with the position of the profile section taken for this study. The grain has a bright core with high Cr and light rim with high Al. b) Graph showing elemental change in a.p.f.u. from core of primary chromite (Chr) grain to the rim of green spinel (GSpl) of the profile section shown in (a) with a gradual change of composition.

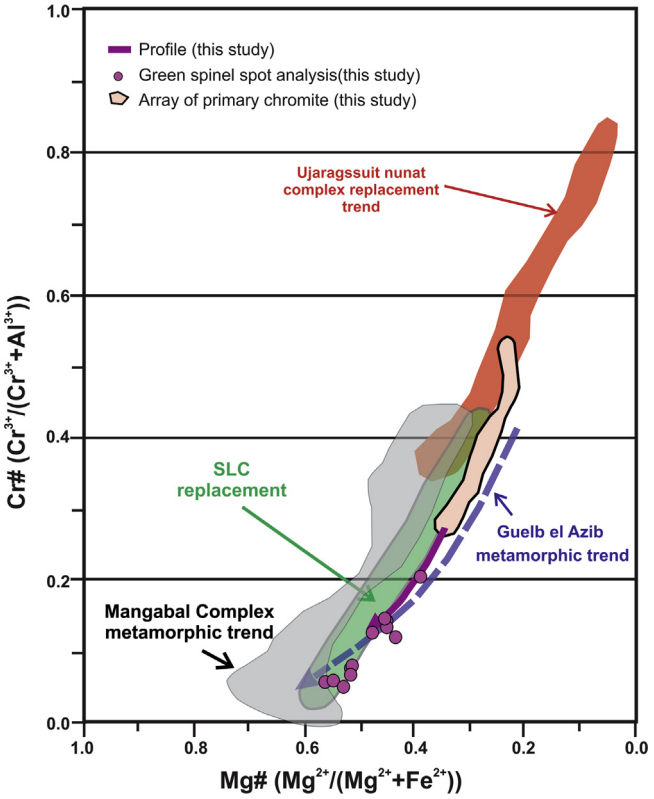

Fig. 10. Mg# vs. Cr# plot with the position of primary chromites and secondary chrome spinel along with the compositional array of data taken from chromite core to the rim of a profile section taken from a single grain shown in Fig. 9a showing the replacement trend. The different metamorphic and replacement trends reported from Archaean chromite deposits similar to the reported trend of this study is also shown in the plot (reference are same as Fig. 8).

melt formed anorthosite having highly calcic plagioclase at temperature >1100 °C. Subsequently, the residual liquid became rich in Fe, Al and Cr and produced Fe-Al rich chromitite seams within clinopyroxenite. Barring the clinopyroxene, the crystallization sequence presented here matches with the same reported by Rollinson et al. (2010) from the Fiskenæsset complex. SLC does not expose of olivine + pyroxene rich cumulate rock although these rocks are plentiful in BLC (reviewed in Dutta et al., 2011). Based on geochemical and isotopic signatures, Bhaskar Rao et al. (1996) proposed that BLC and SLC are genetically and temporally equivalent. Lack of olivine + pyroxene rich cumulates in the SLC could mean that the lower part of the SLC is still not exposed. Presence of dunite, websterite and clinopyroxenite xenoliths in the intrusive felsic rocks supports the view that the SLC is floored with olivine + pyroxene rich rocks (reviewed in Dutta et al., 2011).

6.2. Status of clinoamphibole in the studied rock

There exists a controversy on the origin of amphibole (igneous vs. metamorphic) in the Archaean layered anorthosite complex associated with high grade terrane (reviewed in Dutta et al., 2011; Rollinson et al., 2010). On the basis of textural observation (e.g. clinoamphibole relics in chromite and lack of clinopyroxene in the rock), Rollinson et al. (2010) argued that the clinoamphibole owes its origin to magmatic process. Occurrence of magmatic amphibole in many mantle derived rocks supports the contention of Rollinson et al. (2010). Petrographic features that are presented above provide clinching proof in support of metasomatic amphibole that replaced the magmatic clinopyroxene (Figs. 3b–c, 4d and 5). Similar features were also reported by Berger et al. (2013) and Dutta et al. (2011) from the layered magmatic complex of West African craton and from parts of the SLC respectively. The observed replacement texture of clinopyroxene by the secondary amphibole cannot by itself rule out the possibility of formation of amphibole due to melt-clinopyroxene interaction that occurred during late stage of igneous activity. Few observations are important in this regard:

1. Microtextural features support that amphiboles in the studied rocks show very little or no deformation in contrast to highly deformed clinopyroxene. Furthermore, the grains of clinoamphibole are randomly oriented on the polygonal aggregates of plagioclase. These features support the view that the clinoamphibole in the studied rocks is metasomatic in origin.
2. When present gedrite and clino-amphibole are always intertwined suggesting simultaneous growth. Though igneous gedrite has been reported from a few places (e.g. Eriksberg Gabbro by (Claeson and Meurer, 2002), crystallization of gedrite from a highly calcic melt (that crystallized anorthite) seems to be a difficult proposition.
3. The rocks of SLC are complexly deformed and metamorphosed under first granulite facies followed by amphibolites facies condition at ~2.46 Ga (Ram Mohan et al., 2012). During the amphibolites facies metamorphism, pyroxenes in the granulite facies

Table 5
La-ICP-MS data of REE in hornblende (Hbl), clinopyroxene (Cpx) and plagioclase (Pl).

Mineral	Hbl									Cpx					
Texture	Big grains of Am						Am replacing Cpx								
Sample	S135-106	S135-1010	S135-1011	S135-1012	S135-33	S135-34	S135-29	S135-30	S135-32	S135 - 19	S135-20	S135-22	S135-23	S135-24	S135-25
Analysis	Am1	Am2	Am3	Am4	Am8	Am9	Am5	Am6	Am7	Cpx1	Cpx2	Cpx3	Cpx4	Cpx5	Cpx6
La	0.890	1.230	1.130	1.810	1.230	1.390	1.470	1.320	0.820	0.290	0.240	0.370	0.220	0.350	0.350
Ce	3.390	4.350	3.920	6.610	4.340	5.070	5.010	4.880	2.940	1.160	0.920	1.270	1.140	1.470	1.200
Pr	0.480	0.610	0.580	0.980	0.630	0.730	0.760	0.710	0.460	0.360	0.164	0.219	0.250	0.290	0.198
Nd	1.940	2.550	2.480	4.110	3.080	3.530	3.700	3.560	2.220	1.070	0.920	1.330	1.460	1.580	1.060
Sm	0.520	0.590	0.570	1.060	0.750	0.940	0.940	0.940	0.640	0.290	0.280	0.340	0.480	0.520	0.320
Eu	0.420	0.610	0.610	1.060	1.400	1.530	1.840	1.740	1.030	0.490	0.480	0.470	0.800	0.970	0.370
Gd	0.420	0.610	0.510	0.960	0.700	0.860	0.850	0.990	0.570	0.320	0.300	0.390	0.430	0.480	0.310
Tb	0.087	0.136	0.095	0.210	0.171	0.220	0.200	0.240	0.141	0.083	0.077	0.086	0.136	0.130	0.071
Dy	0.480	0.640	0.640	1.220	1.090	1.270	1.420	1.500	1.010	0.450	0.480	0.600	0.890	1.000	0.390
Ho	0.086	0.140	0.111	0.240	0.220	0.270	0.280	0.340	0.210	0.099	0.102	0.112	0.187	0.200	0.082
Er	0.250	0.350	0.370	0.670	0.660	0.810	0.830	0.950	0.570	0.300	0.300	0.290	0.530	0.600	0.210
Tm	0.044	0.051	0.060	0.100	0.094	0.120	0.153	0.166	0.091	0.040	0.042	0.044	0.084	0.081	0.038
Yb	0.240	0.370	0.370	0.650	0.720	0.890	1.110	1.050	0.680	0.310	0.330	0.290	0.550	0.620	0.210

Mineral	Pl								
Sample	S135-107	S135-108	S135-109	S135-1013	S135-1014	S135-41	S135-42	S135-31	S135-35
Analysis	Pl1	Pl2	Pl3	Pl4	Pl5	Pl6	Pl7	Pl8	Pl9
La	0.0780	0.0690	0.2100	0.4800	0.5700	0.2500	0.1250	0.1110	0.0390
Ce	0.1080	0.0970	0.2200	0.5200	0.5900	0.2300	0.1550	0.1670	0.0570
Pr	0.0076	0.0077	0.0093	0.0340	0.0470	0.0220	0.0174	0.0161	0.0050
Nd	0.0138	0.0210	0.0330	0.0460	0.0980	0.0400	0.0410	0.0440	b.d.l
Sm	0.0039	0.0078	b.d.l	0.0106	0.0086	b.d.l	0.0063	0.0048	0.0095
Eu	0.0550	0.0430	0.0690	0.1380	0.1750	0.3400	0.4200	0.2010	0.1030
Gd	0.0024	0.0100	0.0030	0.0270	0.0168	0.0045	b.d.l	0.0068	b.d.l
Tb	0.0007	0.0007	b.d.l	0.0019	b.d.l	0.0011	0.0006	0.0017	0.0039
Dy	b.d.l	0.0030	b.d.l	b.d.l	b.d.l	0.0070	b.d.l	0.0037	b.d.l
Ho	0.0008	b.d.l	b.d.l	0.0043	b.d.l	0.0006	0.0006	0.0019	0.0006
Er	b.d.l	b.d.l	b.d.l	b.d.l	0.0050	b.d.l	b.d.l	0.0056	b.d.l
Tm	0.0008	b.d.l	0.2100	0.0042	b.d.l	0.0006	b.d.l	b.d.l	0.0025
Yb	0.0032	0.0032	0.0039	0.0170	b.d.l	0.0076	b.d.l	b.d.l	0.0052

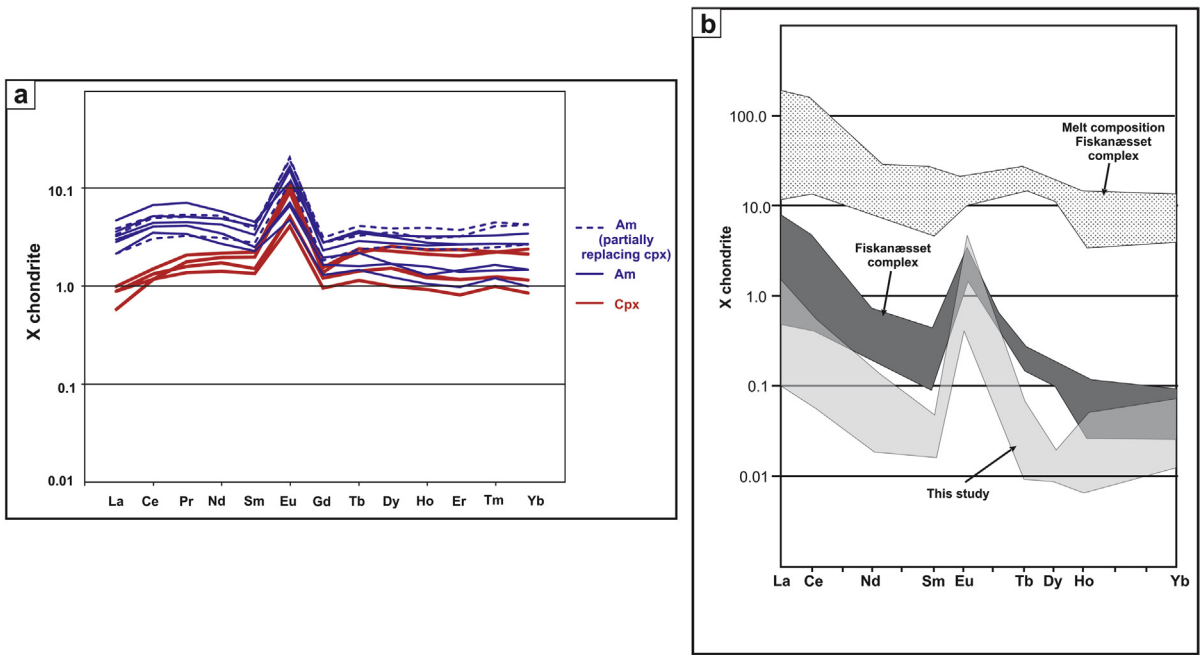

Fig. 11. a) Chondrite normalized REE plots for amphiboles and clinopyroxenes from the chromitite layers of SLC. b) Chondrite normalized REE plots for anorthites from SLC anorthosite of this complex, compared with the anorthites of Fiskenæsset complex and the inferred parental melt composition by Rollinson et al. (2010). The elements incorporated in the plot are exactly similar to Rollinson et al. (2010) whereas the whole range on REE data is given in Table 5.

assemblages in all the rocks are extensively retrograded to amphibole with relicts of pyroxenes. Similar to the amphiboles in the studied rocks, amphiboles in the retrograded granulites formed after the rescission of the major deformation events at the dawn of Proterozoic is already been reported (reviewed in Chowdhury et al., 2013; Ram Mohan et al., 2012).

4. Amphibole of both the categories (replacing clinopyroxene and amphibole from clinopyroxene free area) show indistinguishable REE patters with clinopyroxene which supports the view that the metamorphic amphibole mimics the REE chemistry of the clinopyroxene it replaced.

Combining all the observations it is argued that amphiboles in the studied rocks have metamorphic origin (Berger et al., 2013; Dutta et al., 2011).

6.3. Replacement of chromite by spinel-volume consideration

The compositional variation in Chr and GSpl in the studied chromitite (Section 4.1) can be explained by operation of the exchange vectors $AlCr_{-1}$ and $MgFe_{-1}$. Incidentally, the compositional trend of the altered chromite of this study (Fig. 10) matches with its counterpart in the Ujaragssuit nunat complex of Greenland (Rollinson et al., 2002), Mangabal complex of Brazil (Candia and Gaspar, 1997) and Guelb el Azib complex of West African Craton (Berger et al., 2013). It is argued that the replacement trend of the chromite in the Ujaragssuit nunat complex is a product of interaction of primary chromite with late magmatic liquid (Rollinson et al., 2002) which is not the case in the studied rock. Here a metamorphic origin is supported on the basis of textural evidences. The altered chromite follows a trend that shows a decrease in Fe^{+3}/Al ratio with lower Cr# (Fig. 7). This trend is consistent with the operation of the exchange vector $Al\ (Cr + Fe^{+3})_{-1}$. Similar compositional trend of altered chromite has been reported from the metamorphosed chromitite from the Guelb el Azib complex (Figs. 7 and 10).

Petrographic features show that GSpl retained the shape and size of the Chr it replaced. Hence, the replacement process can be termed as pseudomorphic. Supporting the initial idea of Lindgren (1912), several workers are of the opinion that during pseudomorphic replacement volume remains virtually constant (reviewed in Chowdhury et al., 2013; Hövelmann et al., 2010; Putnis, 2009, 2002; Putnis and Putnis, 2007). This inference leads to the requirement that any pseudomorphic reaction should be balanced on volume (reviewed in Putnis, 2009). Contrary to the extant opinion, Ferry (2000) contented that during pseudomorphic replacement, volume does not remain constant. The change of the solid molar volumes of the parent and the pseudomorph generates strain free energy. If the solid molar volume change of any pseudomorphic reaction becomes negative, the negative strain free energy drives the reaction and helps the pseudomorph to grow (Ferry, 2000). Using this principle, Ferry (2000) explains why the pseudomorph is absent during prograde metamorphism. The idea of Ferry (2000) has been contradicted in subsequent studies that document (a) formation of pseudomorph during prograde metamorphism and (b) solid molar volume of reactant and the pseudomorph remains constant (Dutrow et al., 2008; Dutrow and Henry, 2000). In view of this information it is considered that volume remained virtually constant during the replacement of Chr by GSpl.

6.4. Element mobility during alteration of primary chromite (Chr)-a mass balance approach

Pseudomorphic replacement of Chr by GSpl provides an excellent opportunity to quantify elemental mobility within the volume of an individual grain (Chowdhury et al., 2013; Dutrow et al., 2008, 1999; Hövelmann et al., 2010; Nijland and Touret, 2001).

Philpotts and Ague (2009) derived the following basic equation for calculating the magnitude of relative mass change that occurred during chemical alteration,

$$\Delta C_j = (V^f/V^o)(\rho^f/\rho^o)(C_j^f/C_j^o) - 1 \quad \text{(i)}$$

where ΔC_j– change in concentration of j; where "f" and "o" stands for final and initial compositions; C_j- concentration of 'j', V- volume of the product phase and P- density of phase.

For replacement at constant volume, a likely scenario in pseudomorphism, the equation (i) is reduced to

$$\Delta C_j = (\rho^f/\rho^o)(C_j^f/C_j^o) - 1 \quad \text{(ii)}$$

If "j" remains immobile during the alteration process ΔC_j becomes "0" and equation (ii) turns out to be,

$$C_j^f = (\rho^o/\rho^f)C_j^o \quad \text{(iii)}$$

$$(C_j^f/C_j^o) = (\rho^o/\rho^f) \quad \text{(iv)}$$

In the $C^f/\ C^o$ vs. $(\rho^o/\ \rho^f)$ space equation (iv) defines a line that passes through the origin and have a unit positive slope. This follows that all the elements that remain immobile during the alteration of chromite will lay on the line defined by equation (iv). The mobile element will be plotted above (in case of addition) or below (in case of depletion) the line. The densities of Chr and GSpl have been calculated from the densities of the end-member spinel group of minerals and the stoichiometry of Chr and GSpl (detail procedures are described in Appendix B). Fig. 12a shows the concentrations of different elements that are present in the magmatic chromite (the core of the profile section is treated as initial composition) and Al-rich chrome spinel (the rim of the profile section is treated as final composition). The compositional plot of Fig. 12a shows that the alteration of the magmatic chromite involved the addition of Al and Mg and the loss of Cr and Fe from the chromite grain.

To quantify the absolute loss or gain of different elements equation (i) reorganized to the following form,

$$\Delta C_j\% = [(\rho^{GSpl}/\rho^{Chr})(C_j^{GSpl}/C_j^{Chr}) - 1] * 100 \quad \text{(v)}$$

The superscripts Chr and GSpl refer to the magmatic chromite and altered chrome spinel respectively.

Fig. 11b shows that during alteration of magmatic chromite an increase of MgO by 44 wt% and Al_2O_3 by 40 wt% and a decrease of (Fe_2O_3 + FeO) by 47% and Cr_2O_3 by 32% occurred. In order to understand the source of the added Al and Mg (and fate of the released Fe and Cr) the modelling of the reaction textures around the altered chromite were performed.

6.5. Metamorphic reconstitution and formation of amphibole and spinel

Petrographic observations suggest that spinel and amphiboles developed at the expense of the magmatic assemblage (Chr + plagioclase + clinopyroxene, Fig. 3) during the regional metamorphism. Development of metamorphic amphiboles after the anhydrous magmatic assemblage requires infiltration of fluids into the studied rocks from some external source. Incidentally, infiltration driven metamorphism has been one key feature in the early Palaeoproterozoic regional metamorphism in whole of northern GTSI (reviewed in Brandt et al., 2014; Chowdhury et al., 2013; Raith et al., 2016). Replacement of Chr by GSpl suggests that bonds in the reactant chromite were broken and that Al and Mg were brought to the site of spinel nucleation. Nucleation of GSpl over Chr is, therefore, unlikely to have caused by volume diffusion of Al and Mg into the Chr. Furthermore, Al has very low diffusivity in rocks and minerals under dry condition (Suzuki et al., 2008). The textural features demonstrate that formation of spinel was spatially associated with retrograde amphiboles. Combining all these features it seems logical to assume a fluid mediated process (es) that (a) formed retrograde amphiboles after clinopyroxene and

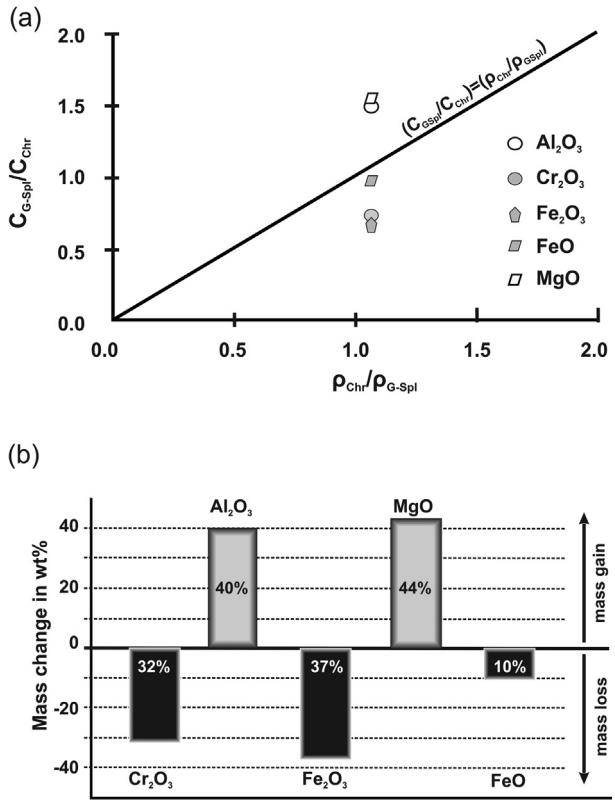

Fig. 12. a) The C_{GSpl}/C_{Chr} vs. ρ_{Chr}/ρ_{GSpl} plot showing elemental mass loss and gain during the pseudomorphic replacement of chromite (Chr) by chrome spinel (GSpl) calculated from the core and rim data of the profile section shown in Fig. 8. During the reaction concentration of elements C_{Chr} changed to C_{GSpl} with the density of the element changing from ρ_{Chr} to ρ_{GSpl}. The line with unit slope stands as the reference line which would have no mass change during the reaction. b) Percentage of mass loss or gain of different individual elements during the pseudomorphism.

plagioclase, (b) transported Al and Mg to the site of spinel, (c) carried Cr and other elements that were present in chromite away from the site of the spinel nucleation and (d) augmented pseudomorphic replacement of Chr by GSpl. Several experimental/theoretical results (Kleine et al., 2014; Wang et al., 1995) and natural observations (Dutrow et al., 2008, 1999; Plümper et al., 2012; Zharikov et al., 2007) convincingly demonstrate that fluid mediated solution (of parent) and reprecipitation (of product phase) process is the key mechanism that controls the growth of pseudomorph in natural rocks (reviewed in Putnis, 2009).

Major compositional difference in spinel and chromite suggests that a number of chemical species were added to and removed from the parent chromite during pseudomorphic replacement. Chemical reactions with solid and ionic species can be balanced in two ways:

(a) on constant volume and (b) on constant compositions of certain chemical species.

For pseudomorphic replacement, balancing chemical reaction on volume seems to be the most logical approach (Dutrow et al., 2008; Hövelmann et al., 2010; Putnis, 2009). In view of this, textural modelling has been done integrating the observed textures and compositions of Chr, GSpl and the associated minerals. The mass balanced reaction that shows minimal volume difference between the reactant Chr and the product GSpl has been chosen. Computer program C-space (Torres-Roldan et al., 2000) has been employed for textural modelling adopted in this study. The detail of the modelling process has been presented in Lang et al. (2004) and Chowdhury et al. (2013). For simplicity, mineral reaction with brown spinel that separates Chr and green spinel in some places has been excluded. Following mass balanced reaction has been considered to explain the spinel pseudomorph:

Employing the above two conditions as filter, following mass balanced reactions are obtained:

$$1114.14\ \mathbf{Chr} + 1433.05\ \mathbf{Pl} + 1622.89\ \mathbf{Cpx} + 877.89\ H_2O + 108.17\ Fe^{2+} + 10.27\ Mn^{2+} + 2328.73\ Mg^{2+} + 370.49\ Na^{+} + 6.03\ K^{+} = 1114.70\ \mathbf{GSpl} + 399.06\ \mathbf{Ged} + 478.82\ \mathbf{Hbl} + 504.04\ SiO_2 + 337.11\ Cr^{3+} + 2152.00\ Ca^{2+} \quad (1)$$

($\Delta V_{\mathbf{Chr\ -\ GSpl}}$ = −2.90%, $\Delta V_{s\%}$ = −7.27%, **loss of Cr** = 70.67 mol%, mineral abbreviation after Kretz, 1983).

The modeled reaction explains a number of textural features such as (a) restriction of GSpl pseudomorph in amphibole rich domains, (b) replacement of clinopyroxene by amphibole and (c) planar boundary between hornblende and gedrite suggesting its textural and chemical equilibrium. Reaction (1) has a negative solid volume change and the difference in volumes between Chr and GSpl is within 3%. The molar volumes of the solid phases are computed with PERPLEX-10 (Connolly, 2005). Within the uncertainties of calculation, <3% volume difference between Chr and GSpl justifies pseudomorphic replacement of the former by the latter mineral. It is to be noted that the modeled reaction predicts immobility of Al but significant mobility of Cr (70.67 mol% loss of Cr) during the formation of GSpl pseudomorph. It is shown in Section 6.4 that formation of GSpl pseudomorph requires significant addition of Al (~40 wt% Al_2O_3) to and loss of Cr (32wt% Cr_2O_3, Fig. 12b) from the pristine Chr. The modeled reaction (1) supports the loss of Cr but conserve Al (i.e. immobility of Al). This apparent riddle can be explained if Al is considered mobile in the scale of a single grain of chromite but immobile in the scale of a thin section. In the latter case, consumption of plagioclase by reaction 1 might supplied the Al required for grain scale transformation of Chr to GSpl. Similar scale dependent behaviour of Al in rocks has been published (Chowdhury et al., 2013). Reaction (1) also suggests that a number of ionic species including Cr were dissolved in the coexisting fluid phase. Since no secondary Cr-bearing phase was seen in the studied rock, it is presumed that the metamorphic fluid transported the Cr for distance more than the size of studied sample. It is commonly perceived that Cr is nominally soluble in crustal and mantle derived fluids and hence it remains immobile in rocks of crustal and mantle origin (Marshall et al., 2003; Watenphul et al., 2014). However, following observations supports the view that Cr can be mobile under certain geological conditions:

(a) Emerald (the sink of Cr and Be) + tourmaline veins in mafic rocks (Marshall et al., 2003).
(b) Emerald-bearing aggregates in ductile shear zone (Schwarz and Giuliani, 2001).
(c) Cr-bearing assemblages in metasomatized rocks of the subduction zone and as inclusion in diamond (reviewed in Klein-BenDavid et al., 2011).

The factors that govern solubility of Cr in geofluids are still not well understood. In surface and ground waters, Cr in high oxidation state (Cr^{6+}) is highly soluble (reviewed in Watenphul et al., 2014). In deep seated condition where the ambient oxidation is not suitable for Cr to be in Cr^{6+} state, solubility of Cr is likely to be governed by some other factors. A number of experimental studies on this issue have demonstrated that pressure and activities of Cl^- and H^+ (particularly the latter) enhance the solubility of Cr^{3+} in crustal and mantle fluids (Klein-BenDavid et al., 2011; Watenphul et al., 2014). Cr^{3+} is least soluble in alkali carbonate and silicate solutions which supports that aqueous fluid is more

efficient carrier of Cr than the carbonic or silicate fluids/liquids (Watenphul et al., 2014). Tracing the source and composition of the infiltrating fluids that caused metasomatism in the studied rock is beyond the purview of this communication. Fe^{2+}/Fe^{3+} ratios in Chr and GSpl (Fig. 7) and in the associated minerals do not support the view that the metasomatic fluid was highly oxidizing so that Cr can be present in 6 + state. That the metasomatic fluid was acidic and aqueous is supported by extensive development of secondary amphiboles over and addition of Fe^{2+} to the magmatic assemblages (reaction 1). Metamorphic pressure of ~11kbar (Chowdhury et al., 2013) also aided the solubility of Cr^{3+} in the fluid. More studies are warranted to decipher the speciation of the soluble Cr species and salinity of the metasomatic fluids.

Acknowledgement

This work was completed during the PhD program of M.T. in the Department of Geological Sciences, Jadavpur University, India and part of the review work was completed in School of Petroleum Technology, Pandit Deendayal Petroleum University, Gandhinagar, Gujarat, India. M.T. acknowledges the financial support of CSIR, India, for funding research fellowship, fieldwork and technical assistance. P.S. and S.S. acknowledge the financial assistance from CAS (Phase VI) granted to Department of Geological Sciences, Jadavpur University and UPE-II program of Jadavpur University supported by University Grants Commission, India. We thank Dhrubajyoti Mukhopadhyay for his valuable opinion on several aspects of this work. We express our gratitude to H. Rollinson, Davide Lenaz and an anonymous reviewer for their thought provoking comments that helped to improve the clarity of the ms. We thank S.K. Mondal for his detail editorial comments.

Appendix A: Analytical method

Chemical composition of the minerals was determined from carbon-coated thin sections of rocks by electron microprobe analysis with JEOL EPMA JXA 8900RL microbeam EPMA at the Mineralogical and Universität zu Köln, Germany and Micro Analyzer at the EPMA Laboratory, Central Petrological Laboratory, Geological Survey of India, Kolkata. At Cologne the instruments were operated at 15 kV accelerating voltage, 1–3 μm beam diameter and 15ηA specimen current. Natural mineral standard were used and the raw data were corrected by PAP procedure (Pouchou and Pichoir, 1984). At the Central Petrological Laboratory, Geological Survey of India, Kolkata, the accelerating voltage used was 15KV with 15ηA current conditions. The beam diameter was 1 μm. The elements were analyzed using natural standards except for Mn and Ti for which synthetic standard was used with an average detection limit of 0.003 wt% for each oxide value.

Selected trace elements were analyzed by Laser Ablation Inductively Coupled Plasma-Mass Spectrometry (LA-ICP-MS) at IIT in Kharagpur using a Cetac 213 nm Nd-YAG laser ablation system connected to a Varian 820 quadrupole ICP-MS. The ablations were done at 10-Hz pulse frequency, 50-μm laser spot size, and 730-V energy. Analyses were performed in peak-hopping mode with each analysis consisting of a 20 s background measurement with the laser turned off, and 40 s peak signal measurement with the laser turned on, during three sequences. Calibration was done using NIST 612 glass and data were reduced using the Glitter© software (Griffin et al., 2008). Other details are been described in Hazarika et al. (2017).

Appendix B: Molar volumes and densities of Chr and GSpl

The molar volumes (V) and densities (ρ) of end members (hornblende, gedrite, anorthite, spinel, hercynite and magnetite) were calculated at 10kbar pressure and 750 °C by PERPLEX-10, a computer program (Connolly, 2005) using the thermodynamic data of Holland and Powell (1998, updated in 2002).

Mineral	Di	An	Ged	Ts/Hbl	Hc	Spl	Mag
Volume (j/mol/bar)	6.72	10.077	25.963	27.025	4.12	4.029	4.559
Density (kg/m^3)					4215.86	3531.228	5078.67

The molecular weight (223.84 gm) and ρ (5.12 gm/c^3) of chromite was obtained from an internet site called "Mindat.org". The primary chromite and the chrome spinel are solid solutions of the four end members from "spinel group of minerals", thus their exact V and ρ were measured by simple formula using their calculated a. p.f.u (atom per formula unit) No. of each element.

$$V_{Chr/GSpl} = \left[(X_{MgAl_2O_4} \times V_{MgAl_2O_4}) + (X_{FeAl_2O_4} \times V_{FeAl_2O_4}) + (X_{FeCr_2O_4} \times V_{FeCr_2O_4}) + (X_{FeFe_2O_4} \times V_{FeFe_2O_4})\right]$$

$$\rho_{Chr/GSpl} = \left[(X_{MgAl_2O_4} \times \rho_{MgAl_2O_4}) + (X_{FeAl_2O_4} \times \rho_{FeAl_2O_4}) + (X_{FeCr_2O_4} \times \rho_{FeCr_2O_4}) + (X_{FeFe_2O_4} \times \rho_{FeFe_2O_4})\right]$$

Therefore finally we used these set of V and ρ for the textural modelling and mass balance calculation respectively:

Mineral	Chr	GSpl (green spinel, profile rim)	GSpl (green spinel)
Volume (j/mol/bar)	4.2043		4.0763
Density (kg/m^3)	4279.42	4021.69	

References

Ashwal, L.D., 1993. Anorthosites. Springer Verlag, Berlin, p. 422.
Ashwal, L.D., Jacobsen, S.B., Myers, J.S., Kalsbeek, F., Goldstein, S.J., 1989. SmNd age of the Fiskenæsset Anorthosite Complex, West Greenland. Earth Planet. Sci. Lett. 91, 261–270. http://dx.doi.org/10.1016/0012-821X(89)90002-2.
Barnes, S.J., Roeder, P.L., 2001. The range of spinel compositions in Terrestrial Mafic and ultramafic rocks. J. Petrol. 42, 2279–2302. http://dx.doi.org/10.1093/petrology/42.12.2279.
Barton Jr., J.M., Fripp, R.E.P., Horrocks, P.C., McLean, N., 1979. The geology, age, and tectonic setting of the Messina Layered Intrusion, Limpopo Mobile Belt, southern Africa. Am. J. Sci. 279, 1108–1134.
Barton, J.M., 1996. The Messina layered intrusion, Limpopo Belt, South Africa: an example of in-situ contamination of an Archaean anorthosite complex by continental crust. Precambr. Res. 78, 139–150.
Berger, J., Diot, H., Lo, K., Ohnenstetter, D., Féménias, O., Pivin, M., Demaiffe, D., Bernard, A., Charlier, B., 2013. Petrogenesis of Archean PGM-bearing chromitites and associated ultramafic-mafic-anorthositic rocks from the Guelb el Azib layered complex (West African craton, Mauritania). Precambr. Res. 224, 612–628. http://dx.doi.org/10.1016/j.precamres.2012.10.005.
Berndt, J., Koepke, J., Holtz, F., 2005. An experimental investigation of the influence of water and oxygen fugacity on differentiation of MORB at 200 MPa. J. Petrol. 46, 135–167. http://dx.doi.org/10.1093/petrology/egh066.

Bhaskar Rao, Y.J., Chetty, T.R.K., Janardhan, A.S., Gopalan, K., 1996. Sm-Nd and Rb-Sr ages and P-T history of the Archean Sittampundi and Bhavani layered meta-anorthosite complexes in Cauvery shear zone, South India: evidence for Neoproterozoic reworking of Archean crust. Contrib. Miner. Petrol. 125, 237–250. http://dx.doi.org/10.1007/s004100050219.

Brandt, S., Raith, M.M., Schenk, V., Sengupta, P., Srikantappa, C., Gerdes, A., 2014. Crustal evolution of the Southern Granulite Terrane, south India: New geochronological and geochemical data for felsic orthogneisses and granites. Precambr. Res. 246, 91–122. http://dx.doi.org/10.1016/j.precamres.2014.01.007.

Candia, M.A.F., Gaspar, J.C., 1997. Chromian spinels in metamorphosed ultramafic rocks from Mangabal I and II complexes, Goias, Brazil. Mineral. Petrol. 60, 27–40.

Chen, C., Su, B.X., Uysal, I., Avci, E., Zhang, P.F., Xiao, Y., He, Y.S., 2015. Iron isotopic constraints on the origin of peridotite and chromitite in the Kizilda?? ophiolite, southern Turkey. Chem. Geol. 417, 115–124. http://dx.doi.org/10.1016/j.chemgeo.2015.10.001.

Chowdhury, P., Talukdar, M., Sengupta, P., Sanyal, S., Mukhopadhyay, D., 2013. Controls of P-T path and element mobility on the formation of corundum pseudomorphs in Paleoproterozoic high-pressure anorthosite from Sittampundi, Tamil Nadu, India. Am. Mineral. 98, 1725–1737. http://dx.doi.org/10.2138/am.2013.4350.

Claeson, D.T., Meurer, W.P., 2002. An occurrence of igneous orthorhombic amphibole, Eriksberg gabbro, southern Sweden. Am. Mineral. 87, 699–708.

Connolly, J.A.D., 2005. Computation of phase equilibria by linear programming: a tool for geodynamic modeling and its application to subduction zone decarbonation. Earth Planet. Sci. Lett. 236, 524–541. http://dx.doi.org/10.1016/j.epsl.2005.04.033.

Dutrow, B.L., Foster, C.T., Henry, D.J., 1999. Tourmaline-rich pseudomorphs in sillimanite zone metapelites: demarcation of an infiltration front. Am. Mineral. 84, 794–805.

Dutrow, B.L., Foster, C.T., Whittington, J., 2008. Prograde muscovite-rich pseudomorphs as indicators of conditions during metamorphism: an example from NW Maine. Am. Mineral. 93, 300–314. http://dx.doi.org/10.2138/am.2008.2621.

Dutrow, B.L., Henry, D.J., 2000. Complexly zoned fibrous tourmaline, Cruzeiro mine, Minas Gerais, Brazil: a record of evolving magmatic and hydrothermal fluids. Can. Mineral. 38, 131–143. http://dx.doi.org/10.2113/gscanmin.38.1.131.

Dutta, U., Bhui, U.K., Sengupta, P., Sanyal, S., Mukhopadhyay, D., 2011. Magmatic and metamorphic imprints in 2.9Ga chromitites from the Sittampundi layered complex, Tamil Nadu, India. Ore Geol. Rev. 40, 90–107. http://dx.doi.org/10.1016/j.oregeorev.2011.05.004.

Elardo, S.M., McCubbin, F.M., Shearer Jr., C.K., 2012. The origin of Chromite Symplectites in Lunar Troctolite 76535: a new look at an old rock. In: 43rd Lunar and Planetary Science Conference 1028.

Feig, S.T., Koepke, J., Snow, J.E., 2006. Effect of water on tholeiitic basalt phase equilibria: an experimental study under oxidizing conditions. Contrib. Miner. Petrol. 152, 611–638. http://dx.doi.org/10.1007/s00410-006-0123-2.

Ferry, J.M., 2000. Patterns of mineral occurence in metamorphic rocks. Am. Mienral. 85, 1573–1588. http://dx.doi.org/10.2138/am-2000-11-1201.

Ghosh, J.G., de Wit, M.J., Zartman, R.E., 2004. Age and tectonic evolution of Neoproterozoic ductile shear zones in the Southern Granulite Terrain of India, with implications for Gondwana studies. Tectonics 23. http://dx.doi.org/10.1029/2002TC001444.

Griffin, W.L., Powell, W.J., Pearson, N.J. and O'Reilly, S.Y., 2008. Glitter: Data reduction software for laser ablation ICP-MS. In Sylvester, P.J. (ed.), Laser Ablation ICP-MS in the Earth Sciences: Current Practices and Outstanding Issues, Mineralogical Association of Canada Short Course Series, Vancouver, B.C., 40, pp. 307–311.

Hazarika, P., Upadhyay, D., Pruseth, K.L., 2017. Episodic tourmaline growth and re-equilibration in mica pegmatite from the Bihar Mica Belt, India: major- and trace-element variations under pegmatitic and hydrothermal conditions. Geol. Mag. 154, 1–19. http://dx.doi.org/10.1017/S0016756815000916.

Holland, T.J.B., Powell, R., 1998. An internally consistent thermodynamic data set for phases of petrological interest. J. Metamorph. Geol. 16, 309–343. http://dx.doi.org/10.1111/j.1525-1314.1998.00140.x.

Hor, A.K., Hutt, D.K., Smith, J.V., Wakefield, J., Windley, B.F., 1975. Petrochemistry and mineralogy of early Precambrian anorthositic rocks of the Limpopo Belt, southern Africa. Lithos 8, 297–310.

Hövelmann, J., Putnis, A., Geisler, T., Schmidt, B.C., Golla-Schindler, U., 2010. The replacement of plagioclase feldspars by albite: observations from hydrothermal experiments. Contrib. Miner. Petrol. 159, 43–59. http://dx.doi.org/10.1007/s00410-009-0415-4.

Klein-BenDavid, O., Pettke, T., Kessel, R., 2011. Chromium mobility in hydrous fluids at upper mantle conditions. Lithos 125, 122–130.

Kleine, B.I., Skelton, A.D.L., Huet, B., Pitcairn, I.K., 2014. Preservation of Blueschist-facies Minerals along a Shear Zone by Coupled Metasomatism and Fast-flowing CO_2-bearing Fluids. J. Petrol. 55, 1905–1939. http://dx.doi.org/10.1093/petrology/egu045.

Kretz, R., 1983. Symbols for rock-forming minerals. Am. Mineral. 68, 277–279.

Lang, H.M., Wachter, A.J., Peterson, V.L., Ryan, J.G., 2004. Coexisting clinopyroxene/spinel and amphibole/spinel symplectites in metamroctolites from the Buck Creek ultramafic body, North Carolina Blue Ridge. Am. Mineral. 89, 20–30.

Leake, B.E., Wooley, A.R., Arps, C.E.S., Birch, W.D., Gilbert, M.C., Grice, J.D., Hawthorne, F.C., Kato, A., Kisch, H.J., Krivovichev, V.G., Linthout, K., Laird, J., Mandarino, J.A., Maresch, W.V., Nickel, E.H., Rock, N.M.S., Schumacher, J.C., Smith, Stephenson, N.C.N., Ungaretti, L., Whittaker, E.J.W., Youshi, G., 1997. Nomenclature of amphiboles: report of the subcommittee on amphiboles of the International Mineralogical Association, Commission on new minerals and mineral names. Am. Mineral. 82, 1019–1037.

Leake, B.E., Woolley, A.R., Birch, W.D., Burke, E.A.J., Ferraris, G., Grice, J.D., Hawthorne, F.C., Kisch, H.J., Krivovichev, V.G., Schumacher, J.C., Stephenson, N.C.N., Whittaker, E.J.W., 2004. Nomenclature of amphiboles: additions and revisions to the International Mineralogical Association's amphibole nomenclature. Am. Mineral. 89, 883–887.

Lenaz, D., Adetunji, J., Rollinson, H., 2014. Determination of Fe^{3+}/SFe ratios in chrome spinels using a combined Mössbauer and single-crystal X-ray approach: application to chromitites from the mantle section of the Oman ophiolite. Contrib. Miner. Petrol. 167, 1–17. http://dx.doi.org/10.1007/s00410-013-0958-2.

Lindgren, W., 1912. The nature of replacement. Econ. Geol. 7, 521–535.

Marshall, D., Groat, L., Giuliani, G., Murphy, D., Mattey, D., Ercit, T.S., Wise, M.A., Wengzynowski, W., Eaton, W.D., 2003. Pressure, temperature and fluid conditions during emerald precipitation, southeastern Yukon, Canada: fluid inclusion and stable isotope evidence. Chem. Geol. 194, 187–199. http://dx.doi.org/10.1016/S0009-2541(02)00277-2.

Matveev, S., Ballhaus, C., 2002. Role of water in the origin of podiform chromitite deposits. Earth Planet. Sci. Lett. 203, 235–243. http://dx.doi.org/10.1016/S0012-821X(02)00860-9.

Mondal, S.K., Ripley, E.M., Li, C., Frei, R., 2006. The genesis of Archaean chromitites from the Nuasahi and Sukinda massifs in the Singhbhum Craton, India. Precambr. Res. 148, 45–66. http://dx.doi.org/10.1016/j.precamres.2006.04.001.

Mukherjee, R., Mondal, S.K., Rosing, M.T., Frei, R., 2010. Compositional variations in the Mesoarchean chromites of the Nuggihalli schist belt, Western Dharwar Craton (India): potential parental melts and implications for tectonic setting. Contrib. Miner. Petrol. 160, 865–885. http://dx.doi.org/10.1007/s00410-010-0511-5.

Nijland, G., Touret, L.R., 2001. Replacement of graphic pegmatite by graphic albite-actinolite- clinopyroxene intergrowths (Mjåvatn, southern Norway). Eur. J. Mineral. 13, 41–50. http://dx.doi.org/10.1127/0935-1221/01/0013-0041.

Nozaka, T., Meyer, R., Wintsch, R.P., Wathen, B., 2016. Hydrothermal spinel, corundum and diaspore in lower oceanic crustal troctolites from the Hess Deep Rift. Contrib. Miner. Petrol. 171, 1–14. http://dx.doi.org/10.1007/s00410-016-1266-4.

Philpotts, A., Ague, J., 2009. Principles of Igneous and Metamorphic Petrology. Cambridge University Press, Cambridge, UK.

Plümper, O., Piazolo, S., Austrheim, H., 2012. Olivine pseudomorphs after serpentinized orthopyroxene record transient oceanic lithospheric mantle dehydration (Leka Ophiolite complex, Norway). J. Petrol. 53, 1943–1968. http://dx.doi.org/10.1093/petrology/egs039.

Pouchou, J.L., Pichoir, F., 1984. A new model for quantitative X-ray microanalysis, Part I: application to the analysis of homogeneous samples. La Recherche Aerospatiale 3, 162–192.

Putnis, A., 2002. Mineral replacement reactions: from macroscopic observations to microscopic mechanisms. Mineral. Mag. 66, 689–708. http://dx.doi.org/10.1180/0026461026650056.

Putnis, A., 2009. Mineral replacement reactions. Rev. Mineral. Geochem. 70, 87–124. http://dx.doi.org/10.2138/rmg.2009.70.3.

Putnis, A., Putnis, C.V., 2007. The mechanism of reequilibration of solids in the presence of a fluid phase. J. Solid State Chem. 180, 1783–1786. http://dx.doi.org/10.1016/j.jssc.2007.03.023.

Raith, M.M., Brandt, S., Sengupta, P., Berndt, J., John, T., Srikantappa, C., 2016. Element mobility and behaviour of zircon during HT metasomatism of ferroan basic granulite at Ayyarmalai, South India: evidence for polyphase neoarchaean crustal growth and multiple metamorphism in the Northeastern Madurai Province. J. Petrol. egw057. http://dx.doi.org/10.1093/petrology/egw057.

Ram Mohan, M., Satyanarayanan, M., Santosh, M., Sylvester, P.J., Tubrett, M., Lam, R., 2012. Neoarchean suprasubduction zone arc magmatism in southern India: geochemistry, zircon U-Pb geochronology and Hf isotopes of the Sittampundi Anorthosite Complex. Gondwana Res. 23, 539–557. http://dx.doi.org/10.1016/j.gr.2012.04.004.

Rollinson, H., 1993. Using geochemical data: evaluation, presentation, interpretation. Mineral. Mag. 58, 392. http://dx.doi.org/10.1180/minmag.1994.058.392.25.

Rollinson, H., Adetunji, J., 2015. Chromite in the Mantle Section of the Oman Ophiolite: implications for the tectonic evolution of the Oman Ophiolite 3 Melt compositions inferred from melt inclusion studies. Acta Geol. Sin. 89, 6–9.

Rollinson, H., Appel, P.W.U., Frei, R., 2002. A metamorphosed, early Archaean Chromitite from West Greenland: implications for the genesis of archaean anorthositic chromitites. J. Petrol. 43, 2143–2170.

Rollinson, H., Reid, C., Windley, B., 2010. Chromitites from the Fiskenaesset anorthositic complex, West Greenland: clues to late Archaean mantle processes. Geol. Soc., London, Special Publ. 338, 197–212. http://dx.doi.org/10.1144/SP338.10.

Sajeev, K., Windley, B.F., Connolly, J.A.D., Kon, Y., 2009. Retrogressed eclogite (20 kbar, 1020 °C) from the Neoproterozoic Palghat-Cauvery suture zone, southern India. Precambr. Res. 171, 23–36. http://dx.doi.org/10.1016/j.precamres.2009.03.001.

Schwarz, D., Giuliani, G., 2001. Emerald deposits — a review. Aust. Gemmol. 21, 17–23.

Sengupta, P., Bhui, U.K., Braun, I., Dutta, U., Mukhopadhyay, D., 2009. Chemical substitutions, paragenetic relations, and physical conditions of formation of

högbomite in the Sittampundi layered anorthosite complex, South India. Am. Mineral. 94, 1520–1534. http://dx.doi.org/10.2138/am.2009.3121.
Sengupta, P., Raith, M.M., Kooijman, E., Talukdar, M., Chowdhury, P., Sanyal, S., Mezger, K., Mukhopadhyay, D., 2015. Chapter 20 Provenance, timing of sedimentation and metamorphism of metasedimentary rock suites from the Southern Granulite Terrane, India, 2015.
Siivola, J., Schmid, R., 2007. List of Mineral abbreviations. IUGS Subcommission on the Systematics of Metamorphic Rocks, 1–14.
Sisson, T.W., Grove, T.L., 1993. Experimental investigations of the role of H_2O in calc-alkaline differentiation and subduction zone magmatism. Contrib. Miner. Petrol. 113, 143–166. http://dx.doi.org/10.1007/BF00283225.
Stowe, C.W., 1994. Compositions and tectonic settings of chromite deposits through time. Econ. Geol. 89, 528–546. http://dx.doi.org/10.2113/gsecongeo.89.3.528.
Subramanium, A.P., 1956. Mineralogy and petrology of the Sittampundi complex, Salem district, Madras state, India. Bull. Geol. Soc. Am. 67, 317–389.
Suzuki, A.M., Yasuda, A., Ozawa, K., 2008. Cr and Al diffusion in chromite spinel: experimental determination and its implication for diffusion creep. Phys. Chem. Miner. 35, 433–445. http://dx.doi.org/10.1007/s00269-008-0238-2.
Takagi, D., Sato, H., Nakagawa, M., 2005. Experimental study of a low-alkali tholeiite at 1–5 kbar: optimal condition for the crystallization of high-An plagioclase in hydrous arc tholeiite. Contrib. Miner. Petrol. 149, 527–540. http://dx.doi.org/10.1007/s00410-005-0666-7.
Torres-Roldan, R.L., Garcia-Casco, A., Garcia-Sanchez, P.A., 2000. CSpace: an integrated workplace for the graphical and algebraic analysis of phase assemblages on 32-bit wintel platforms. Comput. Geosci. 26, 779–793. http://dx.doi.org/10.1016/S0098-3004(00)00006-6.
Vernon, H.R., 2004. A Practical Guide To Rock Microstructure. Cambridge University Press. http://dx.doi.org/10.1017/CBO9780511807206.
Wang, Y., Wang, Y., Merino, E., 1995. Pseudomorphic replacement. Science 59, 1559–1570.
Watenphul, A., Schmidt, C., Jahn, S., 2014. Cr(III) solubility in aqueous fluids at high pressures and temperatures. Geochim. Cosmochim. Acta 126, 212–227. http://dx.doi.org/10.1016/j.gca.2013.10.054.
Windley, B.F., Bishop, F.C., Smith, J.V., 1981. Metamorphosed layered igneous complexes in Archaean granulite-gneiss belts. Annu. Rev. Earth Planet. Sci. 9, 175–198.
Yellappa, T., Chetty, T.R.K., Santosh, M., 2016. Precambrian iron formations from the Cauvery Suture Zone, Southern India: implications for sub-marine hydrothermal origin in Neoarchean and Neoproterozoic convergent margin settings. Ore Geol. Rev. 72, 1177–1196. http://dx.doi.org/10.1016/j.oregeorev.2015.05.002.
Zharikov, V.A., Pertsev, N.N., Rusinov, V.L., Callegari, E., Fettes, D.J., 2007. Metasomatism and metasomatic rocks, 17.

Web references

http://www.mindat.org/min-1036.html, last accessed 29.07.2016.